An Analysis of Moisture Fluxes into the Gulf of California

MAN-LI C. WU, SIEGFRIED D. SCHUBERT, MAX J. SUAREZ, AND NORDEN E. HUANG*

Earth Science Directorate, NASA Goddard Space Flight Center, Greenbelt, Maryland

(Manuscript received 12 March 2008, in final form 17 October 2008)

ABSTRACT

This study examines the nature of episodes of enhanced warm-season moisture flux into the Gulf of California. Both spatial structure and primary time scales of the fluxes are examined using the 40-yr ECMWF Re-Analysis data for the period 1980–2001. The analysis approach consists of a compositing technique that is keyed on the low-level moisture fluxes into the Gulf of California. The results show that the fluxes have a rich spectrum of temporal variability, with periods of enhanced transport over the gulf linked to African easterly waves on subweekly (3–8 day) time scales, the Madden–Julian oscillation (MJO) at intraseasonal time scales (20–90 day), and intermediate (10–15 day) time-scale disturbances that appear to originate primarily in the Caribbean Sea–western Atlantic Ocean.

In the case of the MJO, enhanced low-level westerlies and large-scale rising motion provide an environment that favors large-scale cyclonic development near the west coast of Central America that, over the course of about 2 weeks, expands northward along the coast eventually reaching the mouth of the Gulf of California where it acts to enhance the southerly moisture flux in that region. On a larger scale, the development includes a northward shift in the eastern Pacific ITCZ, enhanced precipitation over much of Mexico and the southwestern United States, and enhanced southerly/southeasterly fluxes from the Gulf of Mexico into Mexico and the southwestern and central United States. In the case of the easterly waves, the systems that reach Mexico appear to redevelop/reorganize on the Pacific coast and then move rapidly to the northwest to contribute to the moisture flux into the Gulf of California. The most intense fluxes into the gulf on these time scales appear to be synchronized with a midlatitude short-wave trough over the U.S. West Coast and enhanced low-level southerly fluxes over the U.S. Great Plains. The intermediate (10–15 day) time-scale systems have zonal wavelengths roughly twice that of the easterly waves, and their initiation appears to be linked to an extratropical U.S. East Coast ridge and associated northeasterly winds that extend well into the Caribbean Sea during their development phase. The short (3–8 day) and, to a lesser extent, the intermediate (10–15 day) time-scale fluxes tend to be enhanced when the convectively active phase of the MJO is situated over the Americas.

1. Introduction

Gulf of California moisture surges are a summertime phenomenon in the southwestern United States. They represent an important mechanism in the transport of moisture from the eastern Pacific Ocean through the Gulf of California into the southwestern United States. The importance of the moisture surge to the precipitation over the southwestern United States has been long recognized (e.g., Bryson and Lowry 1955; Green and Sellers 1964; Carleton 1986; Smith and Gall 1989; Adang and Gall 1989). The surge phenomenon has been acknowledged operationally and studied by researchers for more than 30 years (Hales 1972; Brenner 1974; Douglas 1995; Stensrud et al. 1997; Fuller and Stensrud 2000; Higgins et al. 2004). Adams and Comrie (1997) give a comprehensive review of the subject. The gulf surge does not account for the total Gulf of California–eastern Pacific moisture transport into the desert Southwest. Field studies (Badan-Dangon et al. 1991; Douglas 1995) describe mean southerly flow at the northern end of the Gulf of California during July and August, with a low-level jet as a notable characteristic.

The gulf surge may be defined as the development of a strong southerly or southeasterly flow along the Gulf of California, and particularly at Yuma, Arizona. The surge is most often detected in the surface winds at Yuma,

* Current affiliation: National Central University, Jhongli City, Taiwan.

Corresponding author address: Man-Li C. Wu, NASA GSFC/GMAO, 8800 Greenbelt Rd., Greenbelt, MD 20771.
E-mail: man-li.c.wu@nasa.gov

DOI: 10.1175/2008JCLI2525.1

© 2009 American Meteorological Society

but is also seen at upper-air stations. Accompanying the wind shift is an abrupt rise in dewpoint temperature (Hales 1972; Brenner 1974), cooling, and general increase in low cloud and convective activity (Fuller and Stensrud 2000). The increase in low-level moisture helps to destabilize the boundary layer over the deserts of Arizona and promote the development of deep convection (McCollum et al. 1995).

The actual mechanisms for surge initiation and their relationship to the large-scale circulation patterns are unclear (Hales 1972; Brenner 1974). There have been a number of mechanisms proposed for the gulf surge, yet a detailed description of the dynamics of any of these, either in observational or modeling studies, has yet to be provided. Early work (Hales 1972; Brenner 1974) suggests that some sort of convective outflow propagating the length of the Gulf of California might be responsible. This mechanism may be most applicable to surges that originate from mesoscale convective systems that are located midway up the gulf. The influence of tropical easterly waves on surges is suggested by Hales (1972), although the exact mechanisms by which these two features are related are not described. Using output from a mesoscale numerical model and observations, Stensrud et al. (1997) document that out of six observed surge events, five are preceded by the passage of a tropical easterly wave trough across western Mexico. Fuller and Stensrud (2000) have also suggested that a phasing between midlatitude troughs over the western United States and the easterly waves passing the southern gulf may result in the major surges.

While the impact of the Madden–Julian oscillation (MJO) (Madden and Julian 1972) on precipitation over Southeast Asia has been studied extensively (e.g., Wu et al. 2006), its impact over the Americas and, in particular, over the Gulf of California region is less well established. Molinari and Vollaro (2000) showed that westerly wind bursts associated with the convectively active phase of the MJO create an environment favorable for eastern Pacific cyclogenesis and enhanced convection extending as far east as the southwestern Gulf of Mexico. The MJO is also known to modulate east Pacific hurricanes (Maloney and Hartmann 2000), which have been linked to gulf surges (e.g., Douglas and Leal 2003). Higgins and Shi (2001), using 19 years of National Centers for Environmental Prediction–National Center for Atmospheric Research (NCEP–NCAR) reanalysis data (Kalnay et al. 1996), found a strong relationship between the North American Monsoon System (NAMS) precipitation and eastward propagating MJO events. Lorenz and Hartmann (2006) used the NCEP–NCAR reanalysis data to show that the MJO appears to influence NAMS precipitation by modulating the strength of low-level easterly waves that in turn impact Gulf of California moisture surges.

In this study we use 40-yr European Centre for Medium-Range Weather Forecasts (ECMWF) Re-Analysis data (ERA-40) (Uppala et al. 2005) to examine the nature of the full spectrum of subseasonal variability of the warm- eason moisture flux into the Gulf of California. As such, we do not look specifically at the traditionally defined surge events and the mechanisms by which they traverse the Gulf of California—the data are of insufficient spatial resolution to allow that. Instead, we focus more on the nature of the connections between large-scale atmospheric variability and enhanced northward moisture flux into the Gulf of California. Section 2 describes the data and analysis methods. Section 3 describes the results. The discussion and conclusions are given in section 4.

2. Methods and data

The primary data used for this study are the ERA-40 (Uppala et al. 2005) 6-hourly data. The data extend from September 1957 through August 2002. We focus our attention on the satellite era from 1980 through 2001. The fields used here consist of precipitation, moisture transport at 850 hPa, geopotential height at 500 and 200 hPa, wind at different levels of the atmosphere from the surface to 150 hPa, streamlines at 850 hPa, and velocity potential at 200 hPa. While there are well-known biases and trends in the ERA-40 tropical precipitation fields [in particular an increase in rainfall rates after 1991 associated in part with the impacts of volcanic aerosols on the High Resolution Infrared Radiation Sounder radiances; Uppala et al. (2005)], it nevertheless appears that the time variability on subseasonal time scales (our interest here) is well captured in the reanalysis. All the data were provided on a 2.5° latitude by 2.5° longitude grid. For display purposes, we interpolated the data to a $1° \times 1°$ grid.

To evaluate the temporal and spatial evolution of circulation and precipitation patterns associated with the Gulf of California moisture surges, we form composites based on the meridional component of the moisture flux at 850 hPa at the mouth of the gulf (22°N, 110°W) for the summer months, July–September (JAS), although the results are not very sensitive to exact point or area average used for the index. Since we focus on the moisture entering the Gulf of California, we choose a point close to the mouth of the gulf (i.e., 22°N, 110°W), which is different from the more traditional definition of a moisture surge using data at Yuma.

Three different filters are applied to the data. The 3–8-day filter is a symmetric, 4-pole, low-pass, tangent Butterworth filter described in Oppenheim and Schafer (1975). The filter is applied twice, first retaining time scales longer than 3 days and then retaining time scales

longer than 8 days. The bandpass data are obtained by subtracting the two filtered datasets. The same approach is used to obtain the 10–15-day filter and the 20–90-day filter.

We also perform a wavelet analysis. The wavelet analysis methodology is described in Kaiser (1994) and Keinert (2003). The approach is essentially that of an adjustable window Fourier-type spectral analysis. The basic wavelet function that we used is the Morlet wavelet, defined as Gaussian enveloped sine and cosine wave groups with 5.5 waves.

In addition to the wavelet analysis, we also perform a Hilbert spectral analysis (Huang et al. 1998; Wu et al. 1999; Huang and Shen 2005). The Hilbert–Huang transform is an adaptive method designed specially for analyzing data from nonstationary and nonlinear processes. This analysis does not assume any oscillation or wave functions. The frequency is computed from the intrinsic mode functions (IMFs) through a Hilbert transform and the final result is a time–frequency–energy joint distribution, designated as the Hilbert Spectrum. The IMF decomposition or empirical mode decomposition (EMD) is a method to separate the variations according to their time scale in physical temporal space. The basis is generated adaptively, as discussed in detail in Huang et al. (1998, 1999) and Huang and Wu (2008). Essentially, the method consists of using envelopes defined by local maxima and minima and their mean to force any oscillation to be represented as an IMF, which is defined as any function having the same numbers, or at most differing by one, of zero crossing and extrema; and the mean of its upper and lower envelopes must be zero. With this property, the IMF satisfies the necessary condition to have its Hilbert transform producing physically meaningful instantaneous frequency as the time differential of the phase function. A brief comparison between EMD, Fourier transforms, and wavelets is presented in section 3.

3. Results

a. Northward flux of moisture into the Gulf of California

We begin by characterizing the flow associated with enhanced northward moisture flux into the Gulf of California. As discussed above, we do this by forming a composite of the flow during periods when the flux at the mouth of the gulf (22°N, 110°W) exceeds one standard deviation. A t test is carried out at each grid point to test whether the composite anomaly fields are significantly different from zero. In the case of vector fields, the vectors are plotted if either component is significant at the 5% level. The results (Fig. 1a) show that this is associated with a low-level cyclonic circulation (flux) anomaly (here the data are unfiltered but the annual cycle has been removed) and a large region of enhanced precipitation extending from about 12°N northward into the gulf and much of northwestern Mexico and the southwestern United States. Other features of the low-level moisture flux include an anomalous westerly flux in the eastern tropical Pacific (south of 20°N), enhanced southerly flux over the U.S. Great Plains, and weak cyclonic flow off the East Coast. At upper levels (Fig. 1b), there are anomalous troughs at 500 hPa over both coasts of North America and a low over the coast of California into Mexico and the U.S. Southwest. At 200 hPa, the winds show anomalous cyclonic circulation on both coasts (consistent with the 500-hPa troughs).

The above results indicate that the periods of enhanced low-level northward flux into the Gulf of California tend to be associated with large-scale circulation features that encompass much of North America and extend well into the upper troposphere.

We will next focus on the temporal variability of the fluxes. Figure 2 shows a wavelet decomposition (Kaiser 1994; Keinert 2003) of the northward moisture flux at 22°N, 110°W. The results show a rich spectrum of subseasonal variability with substantial variability on synoptic (subweekly), weekly, and monthly time scales. For example, 1980 shows enhanced variability on the 8–16-day time scales, while 1981 shows periods of enhanced subweekly (2–8 day) variability as well as periods of enhanced variability on 30–60-day time scales. There are also considerable year-to-year changes in the subseasonal variability. Compare, for example, the strong subweekly variability throughout 1998 with the much weaker variability on these time scales during 1991. The wavelet power spectrum (not shown), exhibits some evidence of a peak around 4 to 8 days, but little else in the way of enhanced power at other frequencies.

We next turn to the EMD technique described earlier to find out whether we can identify other frequency bands of enhanced power that might not be evident in wavelet or Fourier transform methods. The most fundamental difference between the EMD method and Fourier or wavelet transforms is that EMD, with an adaptive basis, defines frequency by differentiation, while the Fourier and wavelet, with a priori defined bases, define frequency by integral transforms. The integral transform used in Fourier analysis gives mean frequencies as a global property, while the EMD gives the instantaneous frequencies as a local property. As such, EMD should better resolve oscillations that might be buried in integral-transform-based analysis methods.

Figure 3 summarizes the variability in terms of the spectra computed using the EMD method. The spectra

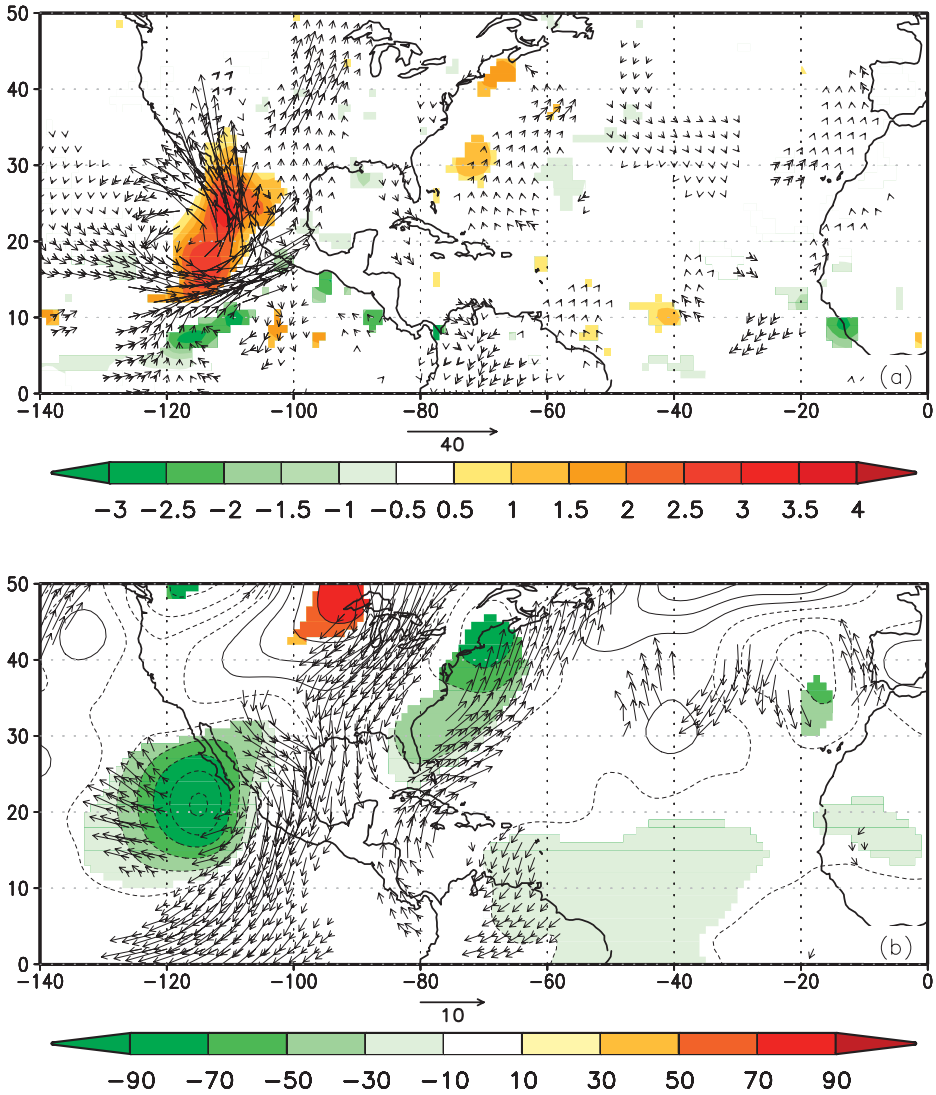

Fig. 1. Composites of anomalies using vq_{850} at 22°N, 110°W as the base point, based on ERA-40 data (1980–2001): (a) Precipitation is shaded with a plotting interval of 0.5 mm day^{-1} starting at ±0.5 mm day^{-1}, and moisture transport (g kg^{-1} m s^{-1}) is at 850 hPa; 5% significant levels are plotted for both precipitation and wind. (b) Geopotential height at 500 hPa is contoured with a plotting interval of 20 m staring at ±10 m (shaded areas are significance at 5% level) and wind (m s^{-1}) is at 200 hPa with significance at 5% level.

are based on 22 years (1980–2001) of vq850 anomalies at 22°N, 110°W during July–October (JASO). We include October in the calculation of the spectra because the standard three-month season calculation is rather marginal for spectrally resolving the longest time scales associated with the MJO (20–90 days) and, in fact, we found that including the extra month helps to better distinguish between the various frequency bands. The spectrum in Fig. 3a reveals evidence for spectral peaks centered near 35, 10, and (to a lesser extent) 5 days. We can also take advantage of the IMF to look at the spectra of subgroups of the leading IMFs. Figure 3b shows that the first IMF peaks in the range 3–8 days and the second in the range 10–15days, while the sum of IMFs 3 through 8 peaks in the range of 20–90 days.

Based on the above analysis of the variability, we look in more detail at the nature and relative contributions to the Gulf of California moisture transport in the three broad spectral ranges consisting of 3–8, 10–15, and 20–90 days. This is justified by the spectra, our inspection of the wavelets, and the IMFs (see above discussion) together with our current understanding of the nature of the variability in this region (in particular, the potential role of easterly waves and MJO—discussed further

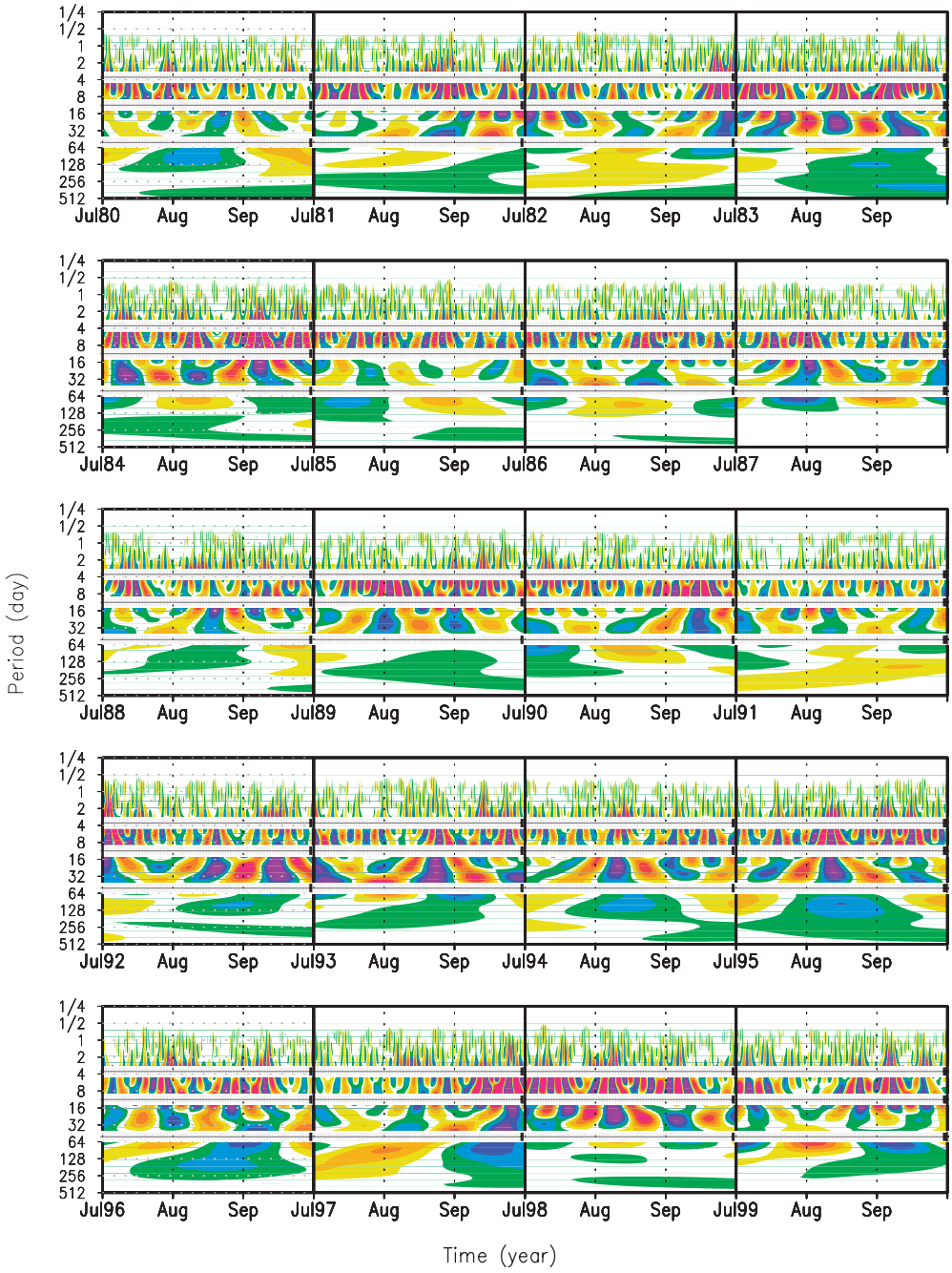

FIG. 2. Wavelets (Morlet) coefficients for vq_{850} at 22°N, 110°W based on ERA-40 data. The plots are for JAS ranging from 1980 through 1999.

below). We note that the 3–8-day band is consistent with our understanding of easterly waves. In particular, Burpee (1975) used Global Atmospheric Research Program Atlantic Tropical Experiment data over western Africa and the eastern Atlantic to analyze the easterly waves and found a dominant frequency between 3 and 8 days.

Our approach is to form composites based on indices of 850-hPa moisture flux that are filtered to retain the three broad spectral ranges mentioned above (see section 2). An alternative approach would be to use the leading (unfiltered) IMFs themselves as indices, though this is somewhat less attractive because the 20–90-day range is made up of several (3–8) of the leading IMFs. In

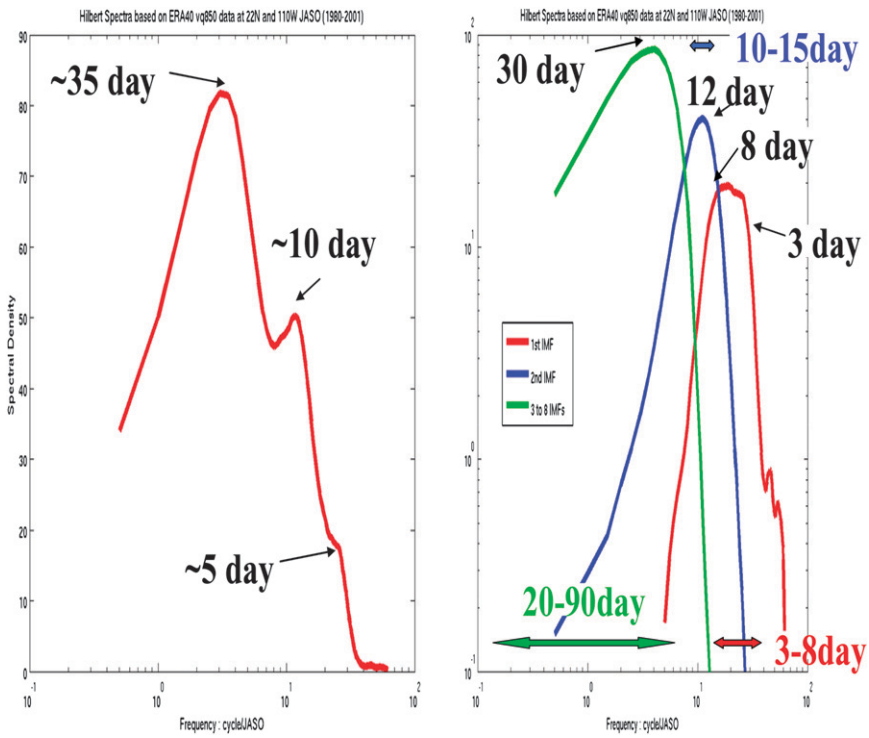

FIG. 3. Marginal Hilbert Spectra for vq_{850} at 22°N, 110°W based on ERA-40 data (1980–2001): (a) Hilbert Spectra of the daily mean anomalies, and (b) Hilbert Spectra of the decomposed intrinsic mode functions.

any event, compositing based on the two leading IMFs (not shown) produced very similar results to those described next for the 3–8- and 10–15-day filter bands.

b. *Link to easterly waves (3–8 day)*

There is considerable evidence that on these time scales (3–8 day) easterly waves play an important role in Gulf of California surges (e.g., Hales 1972), although the exact mechanisms by which they influence the moisture flux into the gulf is not clear. Stensrud et al. (1997) used Hovmöller diagrams of the meridional wind to show the existence of tropical easterly waves around 10° and 22.5°N between 65° and 130°W in connection with gulf surges. Fuller and Stensrud (2000), using 14 years (1979–93) of the ERA-40 dataset, found a total of 85 easterly waves (~3 month^{-1}). A typical wave, with a wavelength of 2500–3800 km, moves from east to west with a speed around 6–8 m s^{-1}. The characteristics of these waves are very similar to those of the waves that have been observed over the eastern Atlantic (Reed et al. 1977). Fuller and Stensrud also found that the easterly waves are intimately tied to the development of gulf surges, with tropical easterly waves passing across western Mexico 1–3 days prior to the onset of gulf surges in Arizona. Higgins et al. (2004), using NCEP–NCAR reanalysis between 1977 and 2001, find that over half of the time the surges are related to the passage of easterly waves.

In the following we look in more detail at the link between the 3–8-day moisture fluxes into the gulf and easterly waves. We note that on these time scales the correlation between the 6-hourly northward moisture flux at our grid point of interest (22°N, 110°W) and the 6-hourly northward moisture flux at the grid point nearest to Yuma is 0.31. This indicates that only a small fraction of the northward moisture flux at the mouth of the Gulf of California actually reaches all the way to Yuma.

Figure 4 shows composites of 850-hPa moisture flux and precipitation anomalies based on data filtered to retain time scales between 3 and 8 days. The index is again the 850-hPa moisture flux at 22°N, 110°W, though in this case everything is based on the filtered data (the composite only includes those time periods for which the filtered northward moisture flux at the base point exceeds one standard deviation). In forming the composites, we have been careful to pick out only the maximum value in the case of consecutive values above the threshold, in order to insure that we are not double counting individual events. The figure also shows time periods before and after the time of maximum northward flux (every 12 hours starting with 2 days

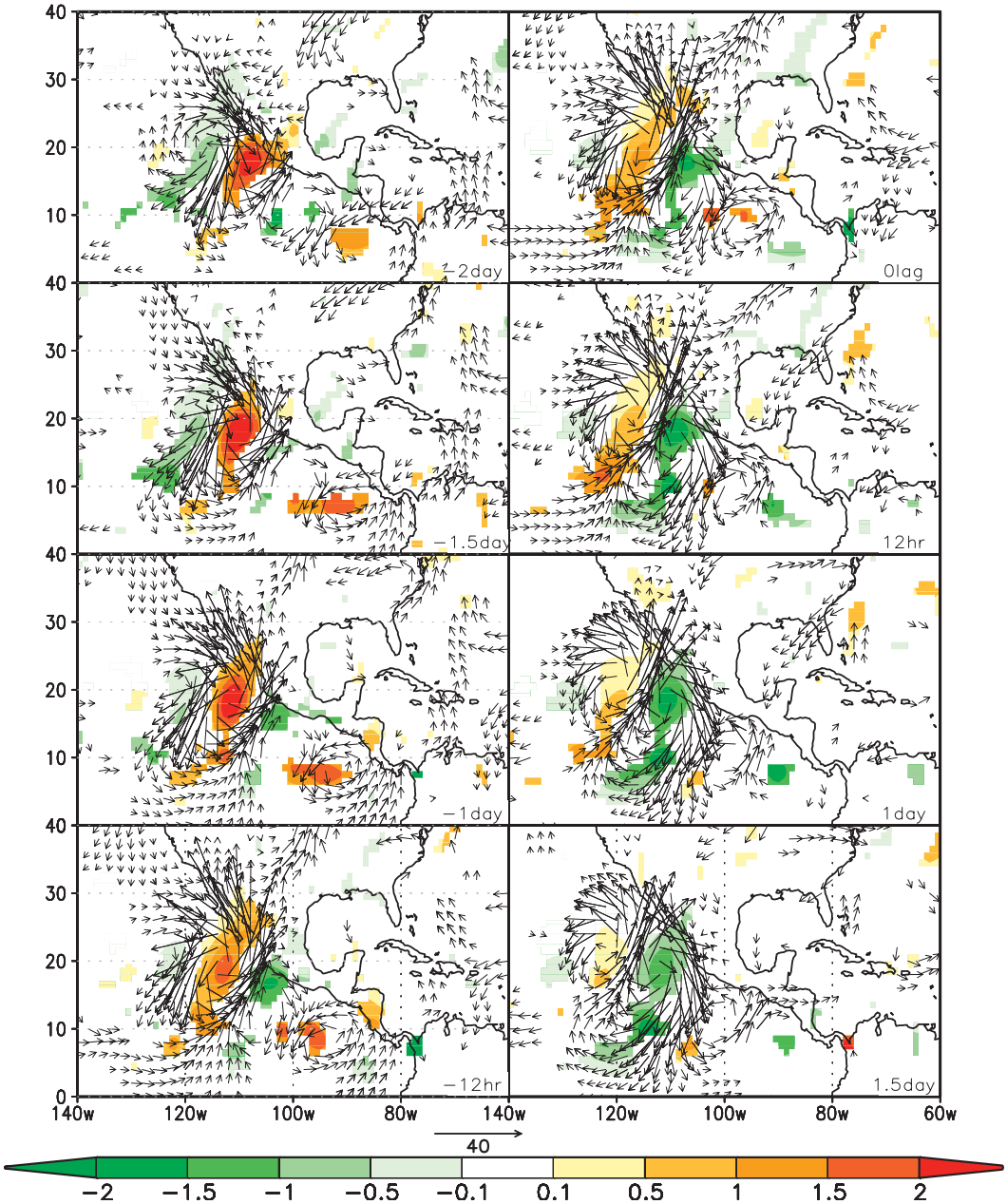

FIG. 4. Composites using vq_{850} at 22°N, 110°W as the base point. Data have a 3–8-day filter applied. Precipitation is shaded with a plotting interval of 0.5 mm day^{-1} starting at ± 0.1 mm day^{-1}, and moisture transport (g kg^{-1} m s^{-1}) is at 850 hPa. The 5% significance levels are plotted for all fields. The plotting time interval is 12 h from the top down and then left to right. All fields plotted have significance at 5% level.

before and ending 1.5 days after the day of maximum flux).

We see in Fig. 4 that, on the day of maximum northward flux (labeled "0lag" in the figure), the transport has a northwest–southeast oriented wave train structure that is characterized by a cyclonic circulation anomaly centered just south and west of the mouth of the Gulf of California, an anticyclonic circulation center to the southeast of that, and another smaller cyclonic circulation center to the southeast of that. The zonal wavelength is about 1500–2000 km. Precipitation is enhanced in the cyclonic centers and suppressed in the anticyclonic center. The enhanced precipitation extends into the gulf and northwestern Mexico. There is also evidence for enhanced northward flux over the central United States. The other panels in Fig. 4 provide a

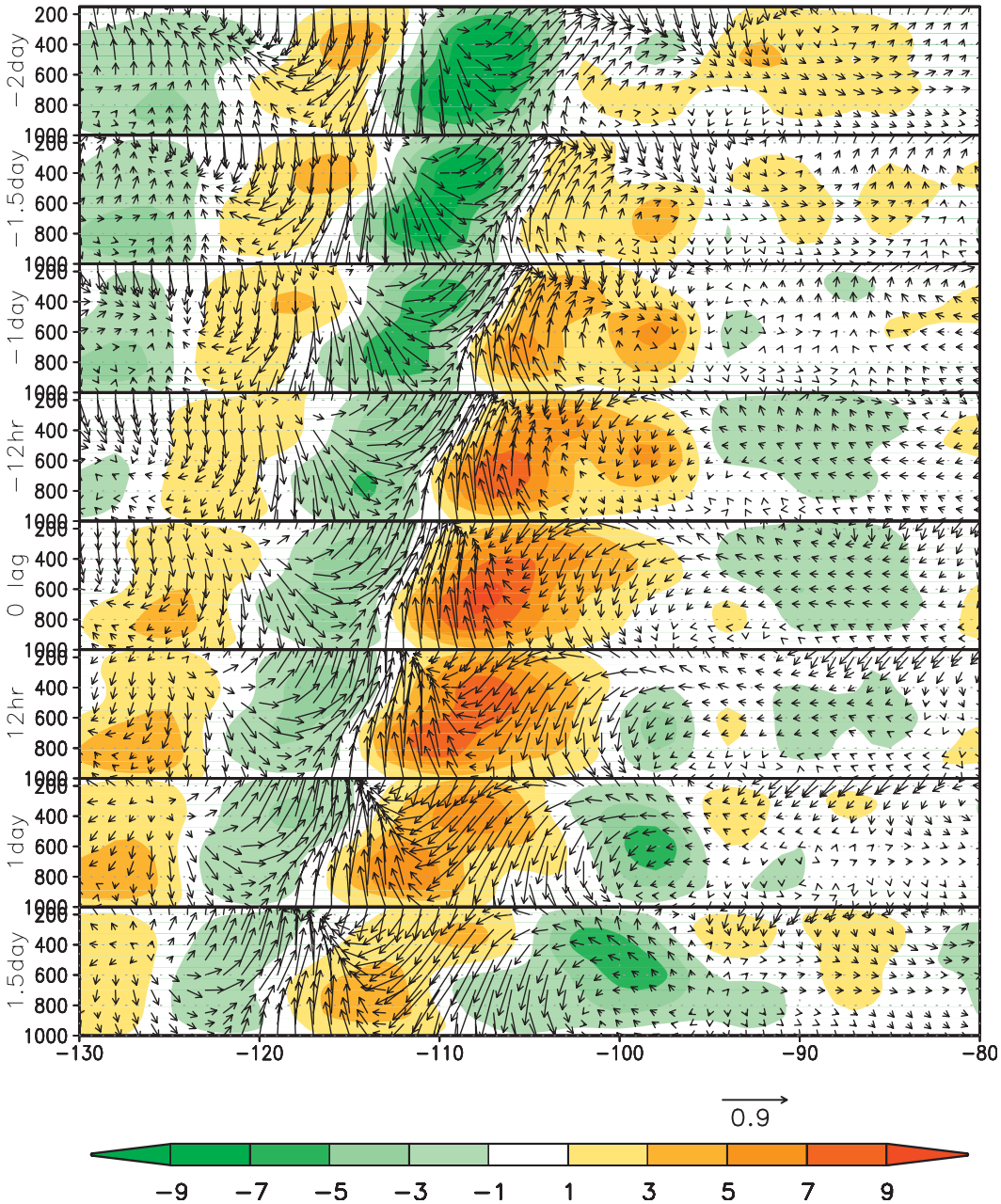

FIG. 5. Longitude–height cross section of composite winds at 17°N using vq_{850} at 22°N, 110°W as the base point. Omega (10^3 Pa s^{-1}) is shaded with a plotting interval of 2×10^3 Pa s^{-1} staring at $\pm 10^3$ Pa s^{-1}. The vectors are the horizontal winds where here a westerly wind is pointing to the right and a southerly wind is point upward. The plotting time interval is 12 h.

sense of the time evolution of the anomalies. Wavelike anomalies are present south of the gulf two days before the maximum flux, and these strengthen and propagate to the northwest until day 0. After day 0, the system moves away from the gulf region to the west-southwest where the anomalies quickly weaken. The fluxes over the central United States oscillate between northerly (day −2), southerly (day 0), and then northerly again at day 1.5.

The vertical distribution of the anomalies (Fig. 5) shows a deep tropospheric layer of southerly winds at the node between coherent and vertically extensive regions of rising and sinking motion. The southerly winds extend well into the upper troposphere, with a

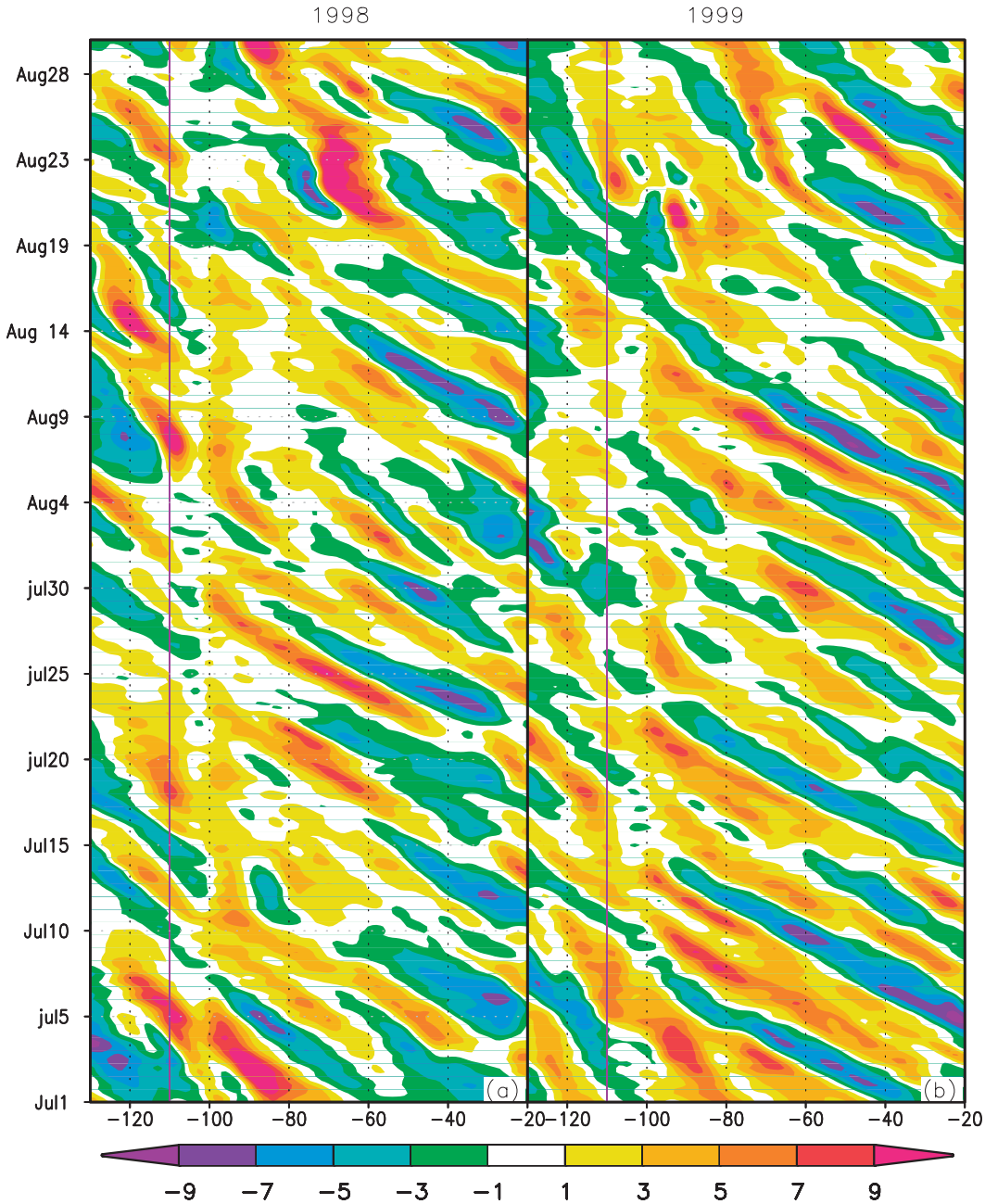

FIG. 6. Hovmöller diagram of the meridional wind (m s^{-1}) at 700 hPa averaged between 20° and 24°N based on ERA-40 data for (a) 1988 and (b) 1999.

wind reversal (northerly flow) occurring at 200 hPa. The region of rising motion is strongest two days prior to the time of maximum flux into the Gulf of California (day 0) and then weakens as the system moves to the west, consistent with the precipitation anomalies shown in Fig. 4. There is a tendency for the rising and sinking motion to show two maxima in the vertical—one near 400 hPa and another around 700 hPa.

We next focus on the link between the above anomalies and easterly waves. Fuller and Stensrud (2000) used Hovmöller diagrams to identify tropical easterly waves. Reed et al. (1977) have shown easterly waves are best defined using wind data at 700 hPa, a result also found in model data by Stensrud et al. (1997). We have found that the waves are easily seen in Hovmöller diagrams of the north–south (v) wind at 700 hPa across the entire latitude belt examined (10°–22.5°N). As an example, we

show in Fig. 6 Hovmöller diagrams of the unfiltered v wind at 700 hPa and 22°N for July–August of 1998 and 1999. The results show clearly the westward propagation of the easterly waves across the Atlantic. Many of them reach all the way into the Caribbean. Some of the waves appear to propagate unimpeded across the Mexican–Central American landmass, while others are disrupted by the land and appear to reform in the Pacific.

Figure 7 shows a sequence of composite fields that attempt to summarize the horizontal structure and basic evolution of the easterly waves. Here the composites are formed from a series of base points that start at 8°N, 20°W and extend across the Atlantic, where the latitude of each subsequent base point (separated by 10° longitude) is determined from the structure of the composite anomalies of the previous base point. The results in Fig. 7 show the waves moving in a somewhat northerly direction crossing over Cuba after which they are disrupted as they hit the Yucatan Peninsula. They tend to reform on the Pacific side somewhat to the south of where they make landfall. We have also done an extended empirical orthogonal analysis of the 700-hPa v wind that provides, from the leading two modes (not shown), a very similar picture of the basic propagation path of the systems. We note that the relevant mechanisms relating easterly waves that develop over the Atlantic Ocean–Caribbean Sea to the development of eastern Pacific tropical cyclones have been described by Zehnder et al. (1999). These involve interactions of the easterly waves with the Sierra Madre and the ITCZ in the eastern North Pacific.

As noted earlier, Fuller and Stensrud (2000) found evidence that major gulf surges were associated with a phasing between midlatitude troughs over the western United States and the easterly waves passing the southern Gulf of California. We look for that here (Fig. 8), by extending our composites into the midlatitudes and showing the 500-hPa height anomalies. The results show the development of a short-wave trough off the West Coast of North America not significant prior to the maximum moisture flux. The trough propagates over the West Coast so that at 1–1.5 days before the time of maximum moisture flux in the gulf, the winds from the midlatitude trough are synchronized with the easterly wave trough and are apparently acting to strengthen it.

c. *Link to intermediate time-scale disturbances (10–15 day)*

Our previous wavelet and spectral analyses indicated that there are contributions to the moisture flux into the Gulf of California on time scales somewhat longer than might be expected from typical weather systems, such as the easterly waves discussed in the previous section. A closer look at Fig. 6 also shows evidence for longer time scales. For example, during 1999 there are a number of time periods when the tendency for northerly winds is maintained for periods of 10 days and longer. In this section we look at these longer time-scale (10–15 day) variations in more detail.

Figure 9 shows the composite evolution of the 850-hPa moisture flux and precipitation anomalies filtered to retain time scales of 10–15 days. The compositing is done in the same way as done in the previous section for the shorter time scales except that the index (the northward 850-hPa moisture flux at 22°N, 110°W) is filtered to retain time scales of 10–15 days (cf. Fig. 4). The lag 0 composite is similar to that shown in Fig. 4 for the easterly wave time scale. The composite also differs in that it shows more extensive regions of easterly and westerly anomalies in the ITCZ and little evidence for flux anomalies over the central United States. The anomalies also tend to be weaker than those associated with the 3–8-day systems. For example, the main wind anomalies in the gulf region are roughly half as large at day 0 as those shown in Fig. 3 for the 3–8-day composites. The time evolution of the anomalies is such that a substantial cyclonic circulation already exists four days earlier at about 15°N (stretching eastward from west of Mexico into the western Gulf of Mexico) producing enhanced precipitation anomalies across much of southern Mexico and the adjacent oceanic regions. In the following days the cyclonic anomaly moves slowly to the west, producing enhanced precipitation across much of Mexico and parts of the southwestern United States and southerly fluxes into the Gulf of California. At the same time, an anticyclonic circulation anomaly and reduced precipitation develop to the south and east of the main cyclonic anomaly. After day 0, the system continues to move westward and weaken. At +3 days, the remnants of the cyclonic circulation are west of 120°W, and the anticyclonic circulation anomaly is situated just south of the Gulf of California, producing northerly flux anomalies in that region together with reduced precipitation that extends across much of Mexico, the Gulf of Mexico, and parts of the southwestern United States.

Figure 10 shows a cross-sectional (longitude–height) view of the evolution of the 10–15-day anomalies: these consist of coherent regions of rising and sinking motion that maximize in the mid to upper troposphere and move slowly to the west. Compared with the synoptic time scales (Fig. 5), the main difference is the larger zonal wavenumber that is manifest at day −3 as a large region of rising motion and southerly winds that extends

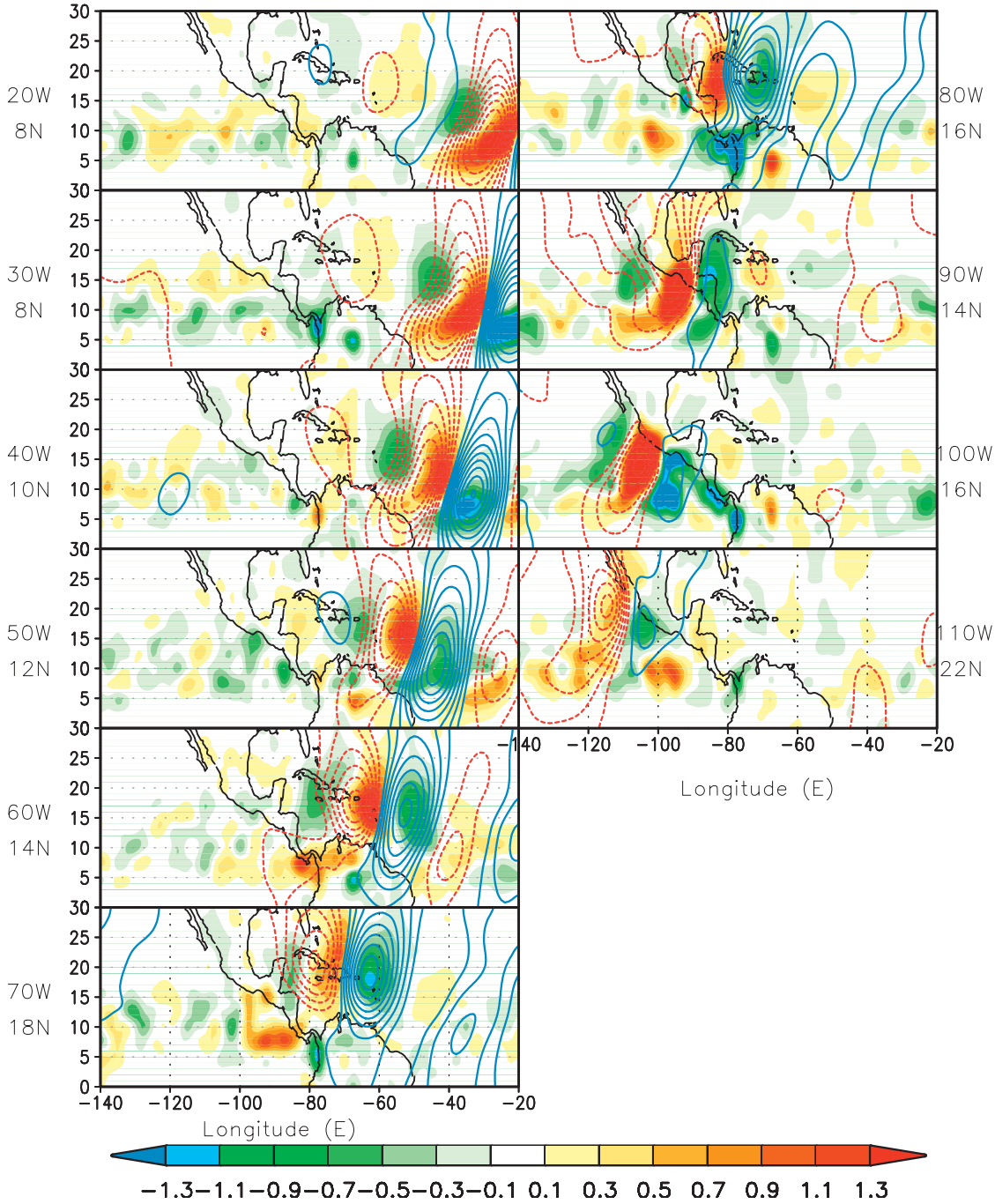

FIG. 7. Composites of precipitation (shaded) and streamline (contour) using vq_{850} at selected locations (marked in the figure) as the base point based on ERA-40 data. The location selection is based on an earlier computation of v_{700} variance (not shown). The maximum v_{700} variance has a southeast–northwest orientation (slope) from the African coast to the U. S. East Coast. The slope is sharper over the eastern Atlantic than over the western Atlantic where it becomes more flat. The streamfunction in Fig. 7 also reveals waves with large southeast–northwest orientation over the eastern Atlantic, and the orientation becomes more flat over the eastern Atlantic. All data have a 3–8-day filter applied (1980–2001). Precipitation plotting interval is 0.2 mm day^{-1} starting at ±0.1 mm day^{-1}.

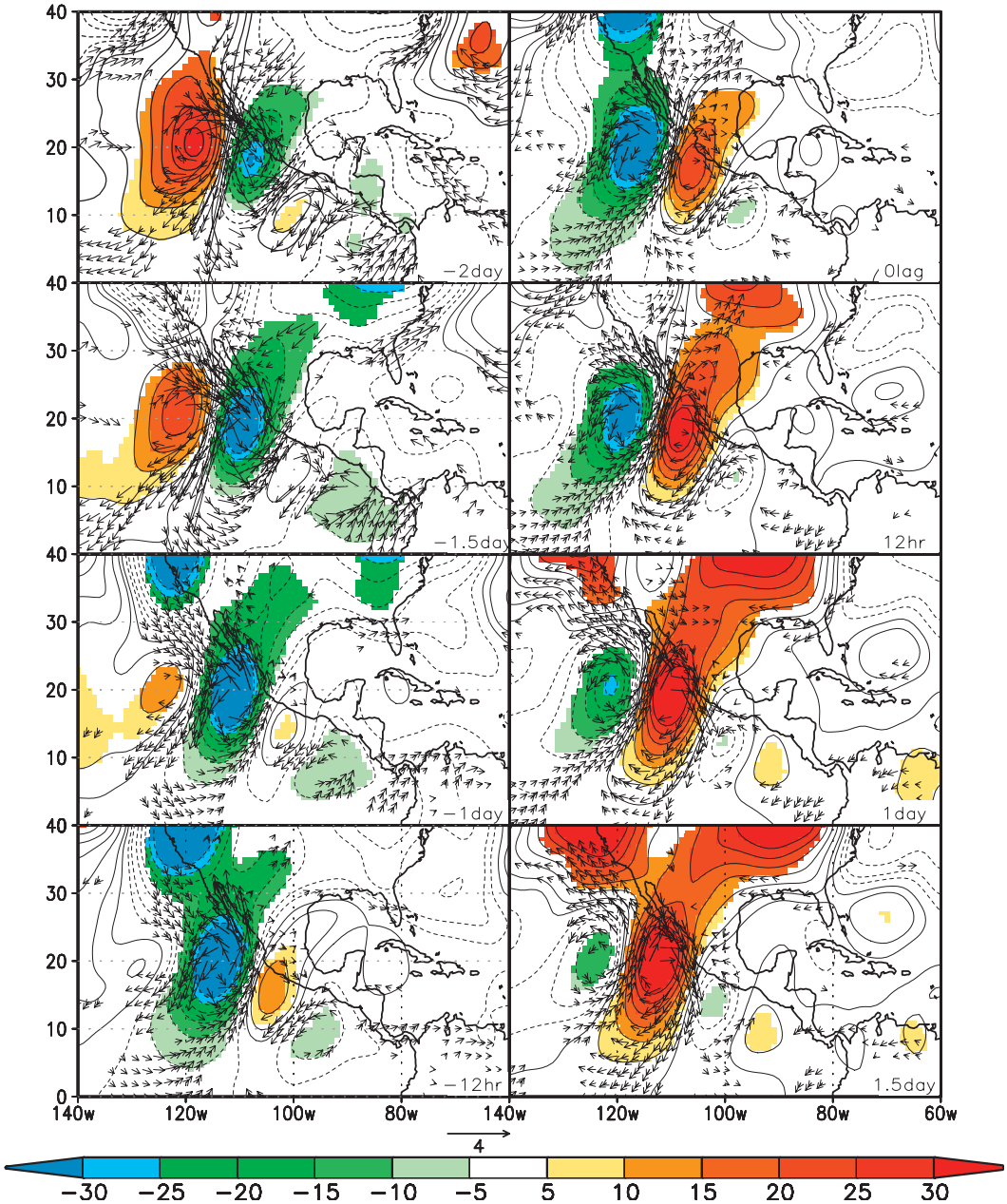

FIG. 8. Composites using vq_{850} at 22°N, 110°W as the base point based on ERA-40 data. All data have a 3–8-day filter applied (1980–2001). Geopotential height (m) is at 500 hPa (contoured; shaded areas have significance at 5% level) and moisture transport is at 850 hPa. The plotting interval for z_{500} is 5 m starting with ±5 m. All fields plotted have significance at 5% level.

across—and is somewhat disrupted by—the continental landmass from the Pacific to the Gulf of Mexico. Similar to the shorter time scales, the southerly winds extend throughout the troposphere, reversing sign only in the upper troposphere. The low-level southerly winds are at a maximum on the leading (east) side of the maximum in rising motion. By day +2 the anomalies are dominated by a large region of sinking motion that, similar to the region of rising motion at day −3, extend across the continental landmass but, in this case, are associated with weak northerly winds extending from the Pacific coast into the Gulf of Mexico.

We have found that the horizontal and vertical structure of the 10–15-day systems is similar to that of the shorter (3–8 day) time-scale systems, though the spatial scales are larger, and some of the details differ. Figure 11

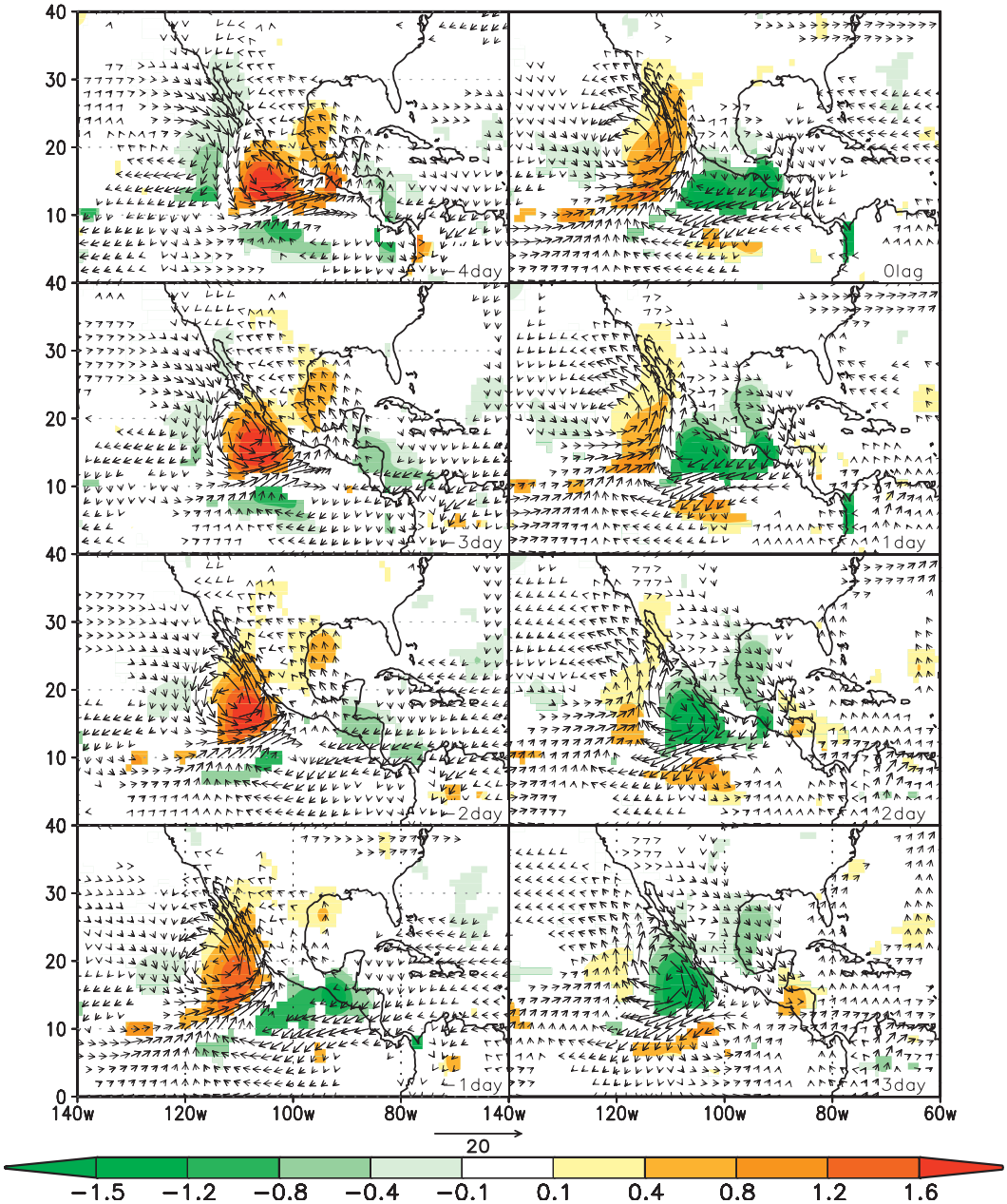

FIG. 9. As in Fig. 4 except that the data have a 10–15-day filter applied. The plotting interval for precipitation is −1.6, −1.2, −0.8, −0.4, −0.1, 0.1, 0.4, 0.8, 1.2, 1.6 mm day^{-1}. The plotting time interval is one day.

compares Hovmöller diagrams of the 850-hPa northward flux of moisture for the two frequency bands during 1983. The 3–8-day fluxes show very clear evidence of the easterly waves propagating across the Atlantic. By comparison, the 10–15-day time scales show less propagation and suggest that the systems (when they are active) tend to originate farther west, especially in the Caribbean Sea. While there is considerable interannual variability in the propagation characteristics, the result overall suggests a weaker link to easterly waves and events in the eastern Atlantic.

There is also some evidence for a link of the 10–15-day systems with the extratropics. Figure 12 shows, for example, composites of the 500-hPa height and the 850-hPa wind anomalies. The result shows that at 4 days there is already an East Coast ridge in place, which is associated with northeasterly winds (at 850 hPa) that extend well into the Caribbean Sea. These winds turn

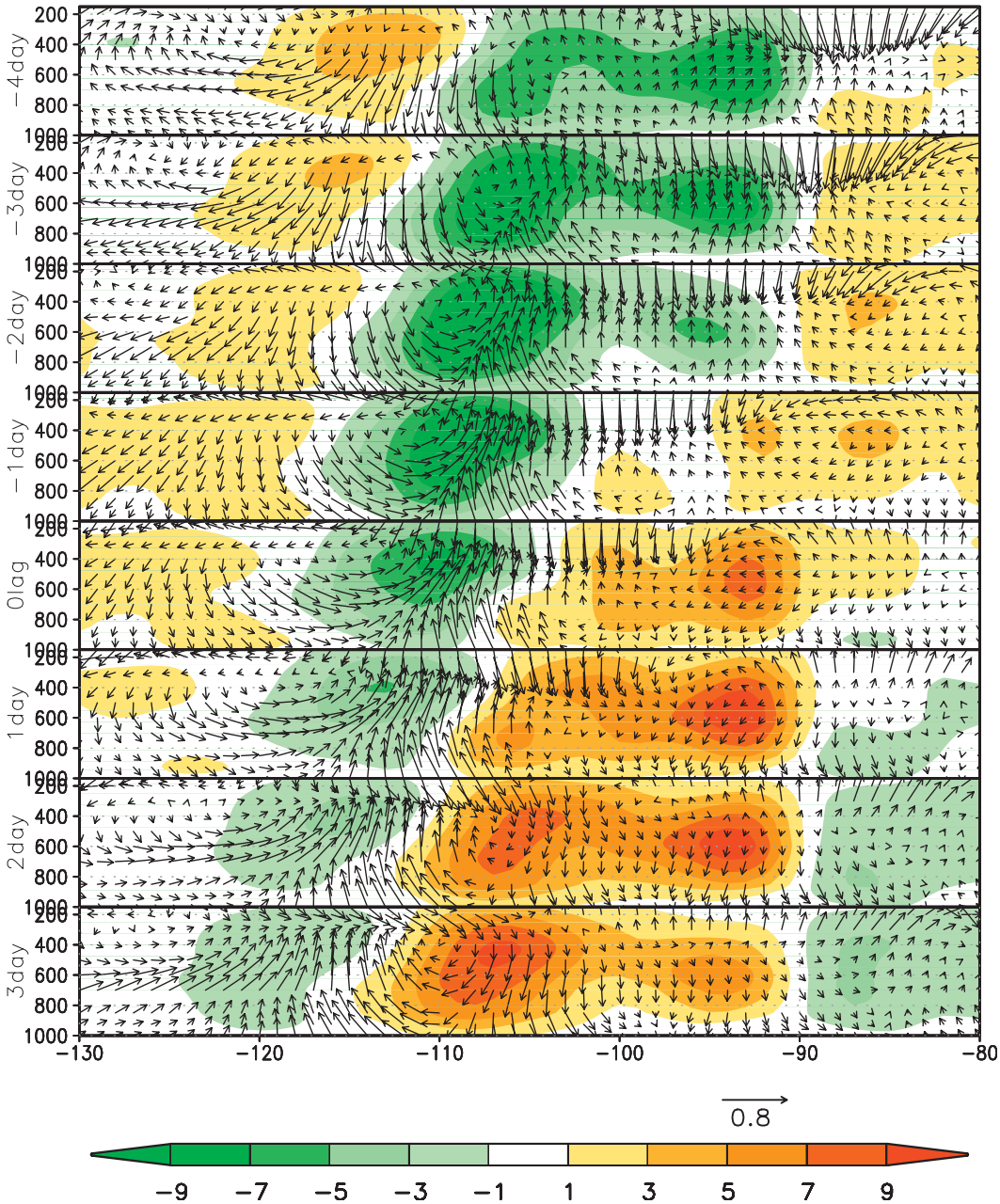

FIG. 10. As in Fig. 5 except that the data have a 10–15-day filter applied. The plotting time interval is one day.

to the northwest and merge with the developing cyclonic system over Mexico. The results suggest that the origin of the 10–15-day systems may be tied to East Coast extratropical systems that extend into the subtropics and Caribbean Sea. Molinari et al. (1997) show that the Charney–Stern necessary condition for instability of the mean flow (it is a condition that the meridional gradient of potential vorticity changes sign over an isentropic surface) is at times met in the Caribbean and speculate that this either invigorates African waves or leads to the actual generation of easterly waves.

Tropical systems similar to those described here have recently been analyzed by Kikuchi and Wang (2009). They found evidence for tropical quasi-biweekly (12–20 day) oscillations that appear to be regional phenomena tied to the different monsoon systems. In particular, they show that the oscillations occur in the Central American monsoon region, where they can be understood in terms of convectively coupled westward-

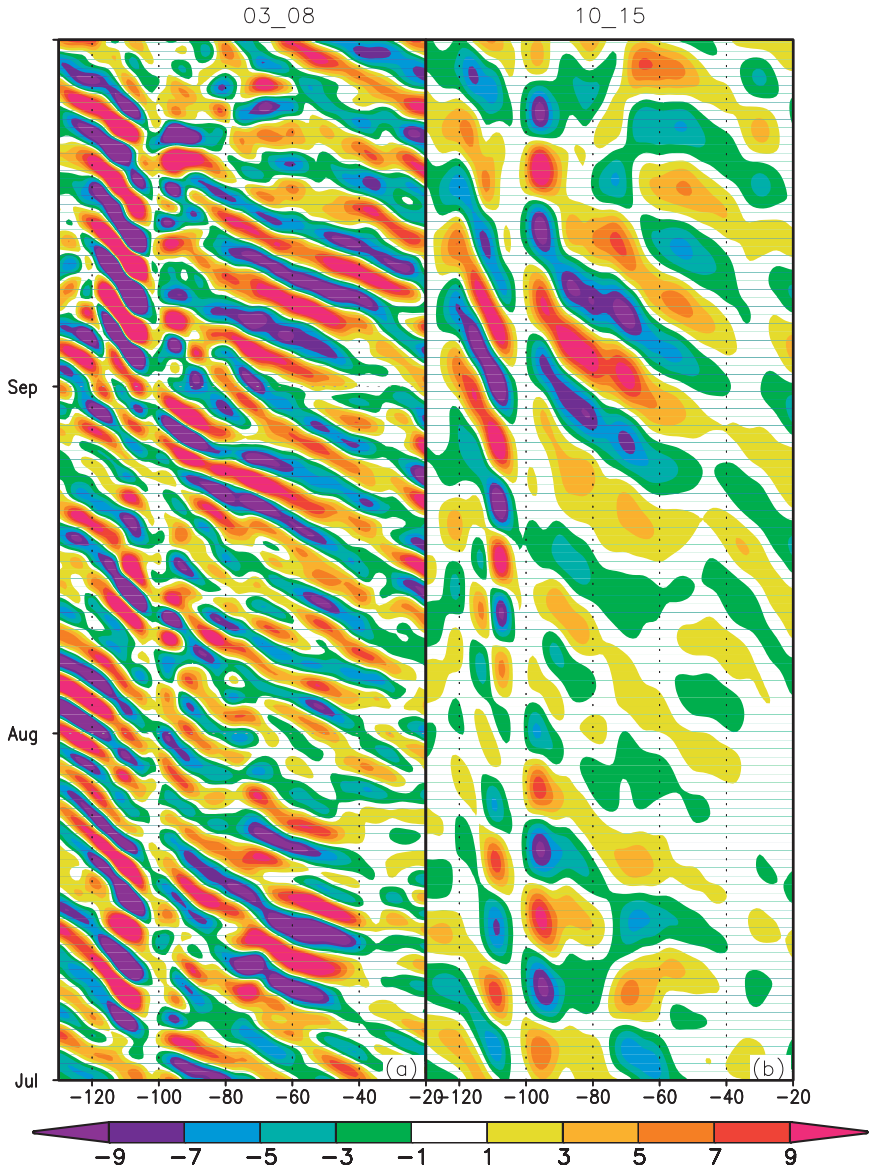

FIG. 11. As in Fig. 6 except that the data have a 10–15-day filter applied.

propagating equatorial Rossby waves in the presence of a mean monsoonal flow. They found that the Central American oscillations have a wavelength of ~70° longitude, a phase speed of ~5 m s^{-1}, and convective activity that is predominantly off equatorial (10°–30° latitude). That is consistent with our results, though in our case the wavelength appears to be closer to 50°–60° longitude (e.g., Fig. 12). Further results concerning the 10–15-day variability are presented in section 3e.

d. Link to the MJO (20–90 day)

As already mentioned, Higgins and Shi (2001) found a strong relationship between the NAMS precipitation and eastward propagating MJO events. Although a combined northward and eastward propagation of the MJO effect is not as strong as that found in the Indian summer monsoon (Wu et al. 2006), they found that the positive polarity of the leading principal component of intraseasonal variability is associated with an intensification and northward adjustment of the precipitation pattern in the eastern tropical Pacific. Furthermore, Lorenz and Hartmann (2006) showed that the MJO appears to influence NAMS precipitation by modulating the strength of low-level easterly waves propagating into the Pacific from the Caribbean Sea, which in turn impact Gulf of California moisture surges. They also

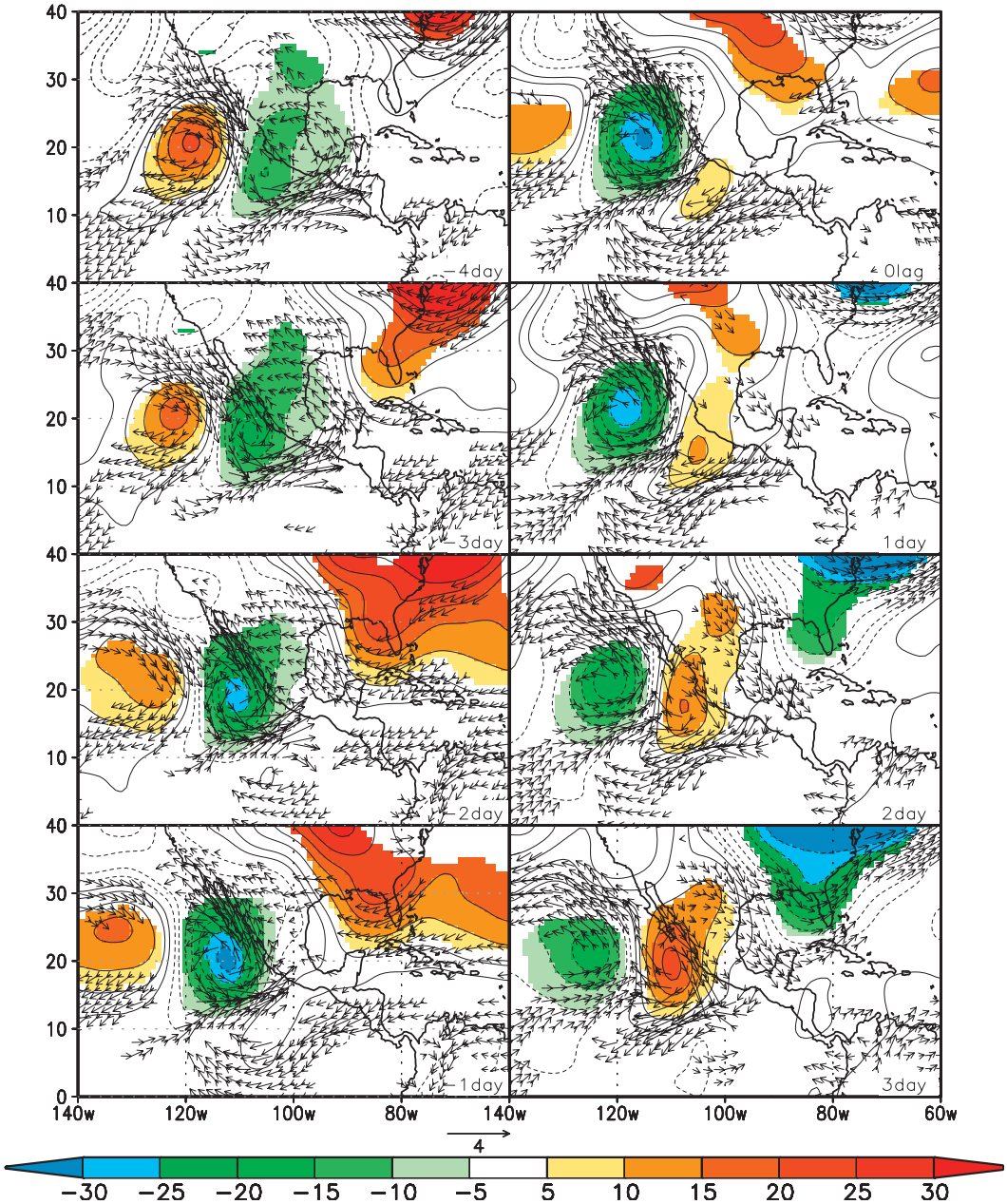

FIG. 12. As in Fig. 8 except that the data have a 10–15-day filter applied. The plotting time interval is one day.

suggest alternative mechanisms in which the MJO impacts tropical cyclones in the eastern Pacific (Maloney and Hartmann 2000), which in turn triggers a gulf surge, or it may be that the westerly MJO anomalies lead to cross-orographic flow that is favorable for mesoscale convective systems. Other studies found that the response of the ITCZ to the easterly wave forcing can result in gulf surge events and also suggest that the response may depend on the phase of the MJO, especially the westerly phase of the MJO (Zehnder et al. 1999; Vera et al. 2006). In this section we look more closely at the moisture fluxes on the MJO time scales (20–90 day) and the link to the MJO.

Figure 13 shows the composites of precipitation and 850-hPa moisture fluxes using the same base point (22°N, 110°W) as was used for the other time scales, but where the index (the moisture flux at 850 hPa) has been filtered to retain only time scales of 20–90 days. In addition, all composite fields are based on data that have been similarly filtered. The results show what is largely

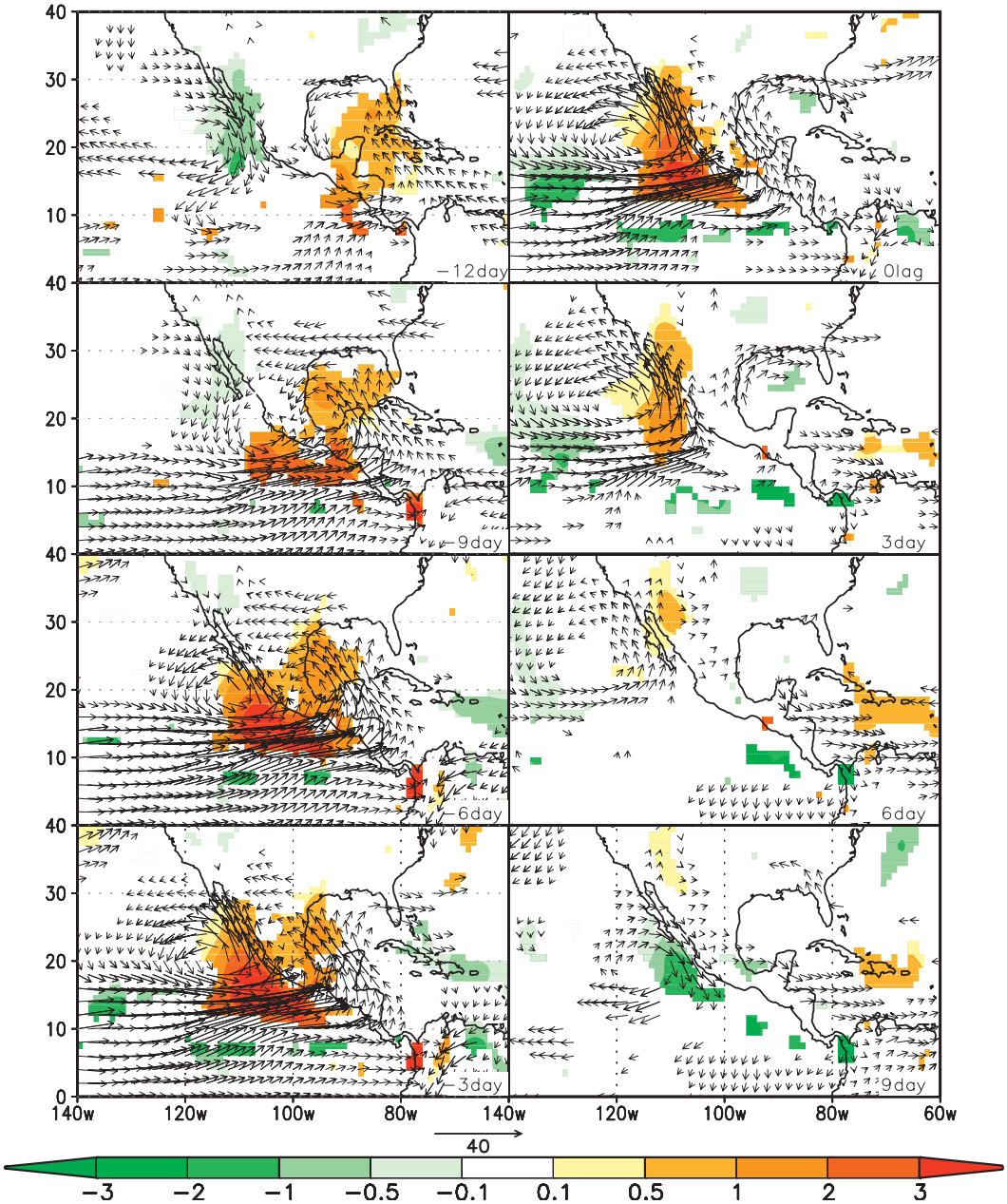

FIG. 13. As in Fig. 4 except that the data have a 20–90-day filter applied. The plotting time interval is 3 days.

an in situ development of strong westerly flux anomalies that peak in the far eastern Pacific between 10° and 15°N a few days before the maximum moisture flux into the Gulf of California. The fluxes are part of a cyclonic circulation anomaly that is well defined by day −9, transporting moisture from the Caribbean into the Gulf of Mexico, with a large region of enhanced precipitation extending from the eastern Pacific, across Mexico, and into the Gulf of Mexico and Caribbean Sea. In the following days, the cyclonic circulation anomaly strengthens and splits, producing (by day −3) two regions of enhanced southeasterly flux and precipitation on either side of Mexico. The cyclonic circulation complex slowly moves to the west and begins to weaken so that by day 0 the southeasterly flux is largest in the eastern Pacific, extending into the Gulf of California with enhanced precipitation covering much of the Gulf of California, the southwestern United States, and northwestern Mexico. By day +3 the southeasterly flux anomalies over the Gulf of Mexico have largely disappeared, and

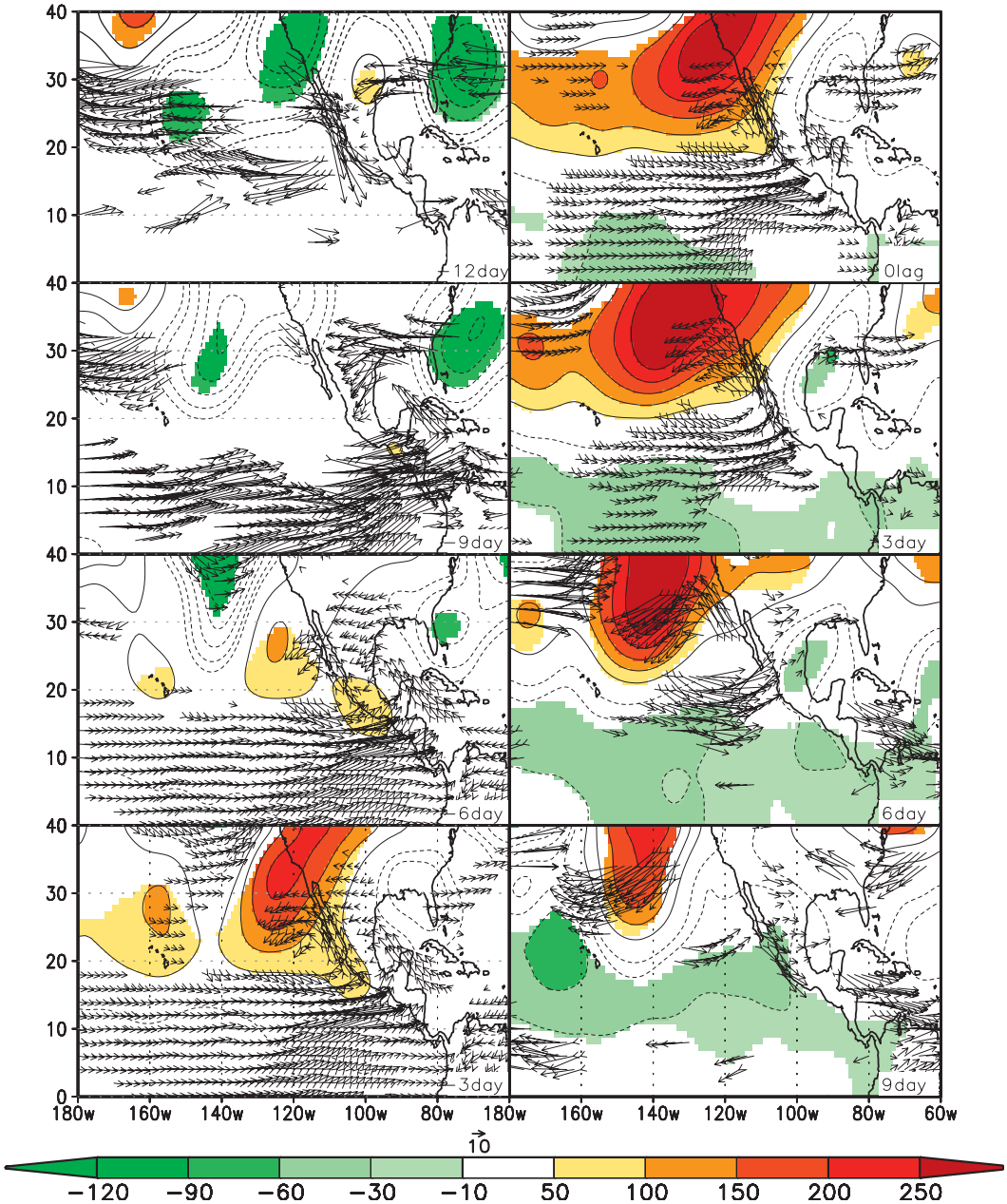

FIG. 14. As in Fig. 5 except that the data have a 20–90-day filter applied. The geopotential height (shaded) is at 200 hPa with a plotting interval of 50 m for positive anomalies and 30 m for negative anomalies. The plotting time interval is 3 days.

the cyclonic circulation anomaly is confined to the eastern Pacific with positive precipitation anomalies confined to regions west of 100°W, and by day +6 the cyclonic circulation anomaly has largely disappeared and only weak precipitation anomalies remain throughout the region. At day +9 we see the development of an anticyclonic flux anomaly just south of the Gulf of California.

The connections with the extratropics on these time scales consist largely of the development of an upper-tropospheric anomalous West Coast ridge and a lower-tropospheric cyclonic circulation anomaly that develops upstream in the North Pacific (Fig. 14). The ridge appears to be a response to the heating associated with the precipitation anomalies in the far eastern tropical Pacific, discussed previously. The anomalous ridge develops at day −6 just west of Baja California. It replaces a weak anomalous trough that is situated in the eastern Pacific prior to that time. By day 0 the anomalous

ridge has strengthened and expanded to cover a substantial part of the Pacific coast and western United States. It then weakens and at day 6 begins to split in two with the western component moving into the Pacific where it decays and the eastern component contributing to weak ridging over the eastern United States. The nature of the low-level cyclonic circulation anomaly in the North Pacific is not clear. It replaces an anticyclonic circulation anomaly in that region prior to day −6. The cyclonic circulation appears to develop in conjunction with the development of the West Coast ridge at day −3 (centered near 40°N, 160°W) and then intensifies and eventually moves westward and weakens. Also noteworthy is the enhanced low-level anticyclonic circulation over the south-central and eastern United States from day 0 to 6, which appears to be a manifestation of an enhanced "conveyer belt" of moisture flux across that region of the country (see also Fig. 13).

While the above composites are based on data filtered to retain time scales between 20 and 90 days, the link to the MJO is not obvious. The development of the main precipitation and moisture flux anomalies appears to be rather stationary, though the development of the strong surface westerly anomalies (e.g., Figs. 13 and 14) does suggest an influence from the MJO. In fact, correlations between an MJO index[1] and the tropical $u_{850\ \mathrm{hPa}}$ at each grid point show the tropical eastern Pacific to have some of the highest correlations (greater than 0.25).

Figure 15 shows the composite fields of the 200-hPa velocity potential, again based on the index consisting of the 850-hPa northward moisture flux at the mouth of the Gulf of California. The results do suggest eastward propagation over the course of 40 days. There appears to be rapid propagation (or even a jump) of weak anomalies across the Pacific followed by an in situ intensification between days −10 and −5 with little, if any, propagation. This behavior likely reflects the fact that the compositing index emphasizes those periods when precipitation anomalies develop in the far eastern Pacific and act to lock the MJO into that region as part of a Rossby wave response to the associated heating (note the westward propagation of the negative anomalies between days −10 and day 0). This is consistent with the development of the low-level flux and precipitation anomalies discussed previously, as in Fig. 13. The results are consistent with the findings of Lorenz and Hartmann (2006), suggesting that the MJO does play a role in the development of the northward moisture fluxes over the Gulf of California on these time scales in providing the large-scale environment (rising motion) and surface westerlies that lead to enhanced precipitation anomalies in the far eastern Pacific.

e. Relationships between the MJO, easterly waves, and intermediate time scales

In the previous sections we examined the nature of the phenomena responsible for enhanced northward flux of moisture into the Gulf of California on three different rather broad time scales (3–8, 10–15, and 20–90 days). This separation of time scales has helped us identify distinct phenomena (storm systems) that, in addition to having different time scales, have different spatial scales, different origins, and differences in their links with the extratropics.

In this section we examine the extent to which the variability in these three frequency bands is related. In particular, we are interested in determining to what extent the shorter time scales are modulated by the 20–90-day variations. Figure 16 shows the time series of the base-point 850-hPa northward moisture flux for the three different filters. In addition to being filtered, the 3–8- and 10–15-day time series have been squared so that we are looking at the changes in amplitude. A broad brush view of these time series shows that there is a tendency for the 3–8- and 10–15-day amplitudes to be largest when the 20–90-day values are large and positive. In fact, if we compute the variances of the 3–8- and 10–15-day squared time series separately based on the polarity of the 20–90-day time series, we find that, when the 20–90-day time series is positive, the 3–8- (10–15) day variances are 2.6 (2.1) times larger than when it is negative.

We have also fit a smooth (spline) envelope curve to the squared time series in Fig. 16 and computed correlations between the 20–90-day time series and the envelope curves. The correlations are 0.42 for the 3–8-day squared time series and 0.23 for 10–15-day squared time series. Furthermore, the correlation between the two squared (envelop) time series is only 0.13.

We interpret the above results as an indication that the MJO (as reflected in the 20–90-day variability) acts to either inhibit or enhance the development of the 3–8- and 10–15-day variability. During those times when the rising branch of the MJO approaches the far eastern Pacific there is a tendency for it to lock in place (become stationary). This is accompanied by the development of enhanced precipitation and cyclonic circulation in a broad region covering the far eastern tropical Pacific and extending across the Americas into the western

[1] Our index is based on that computed by Maloney and Kiehl (2002). It is computed from the two leading principal components of the 30–90-day 850-hPa zonal wind averaged between 5°S and 5°N. Our calculation differs in that the time period is limited to the months of July, August, and September, and the filter retains time scales of 20–90 days. Also, the latitudinal average is done from 5°S to 15°N.

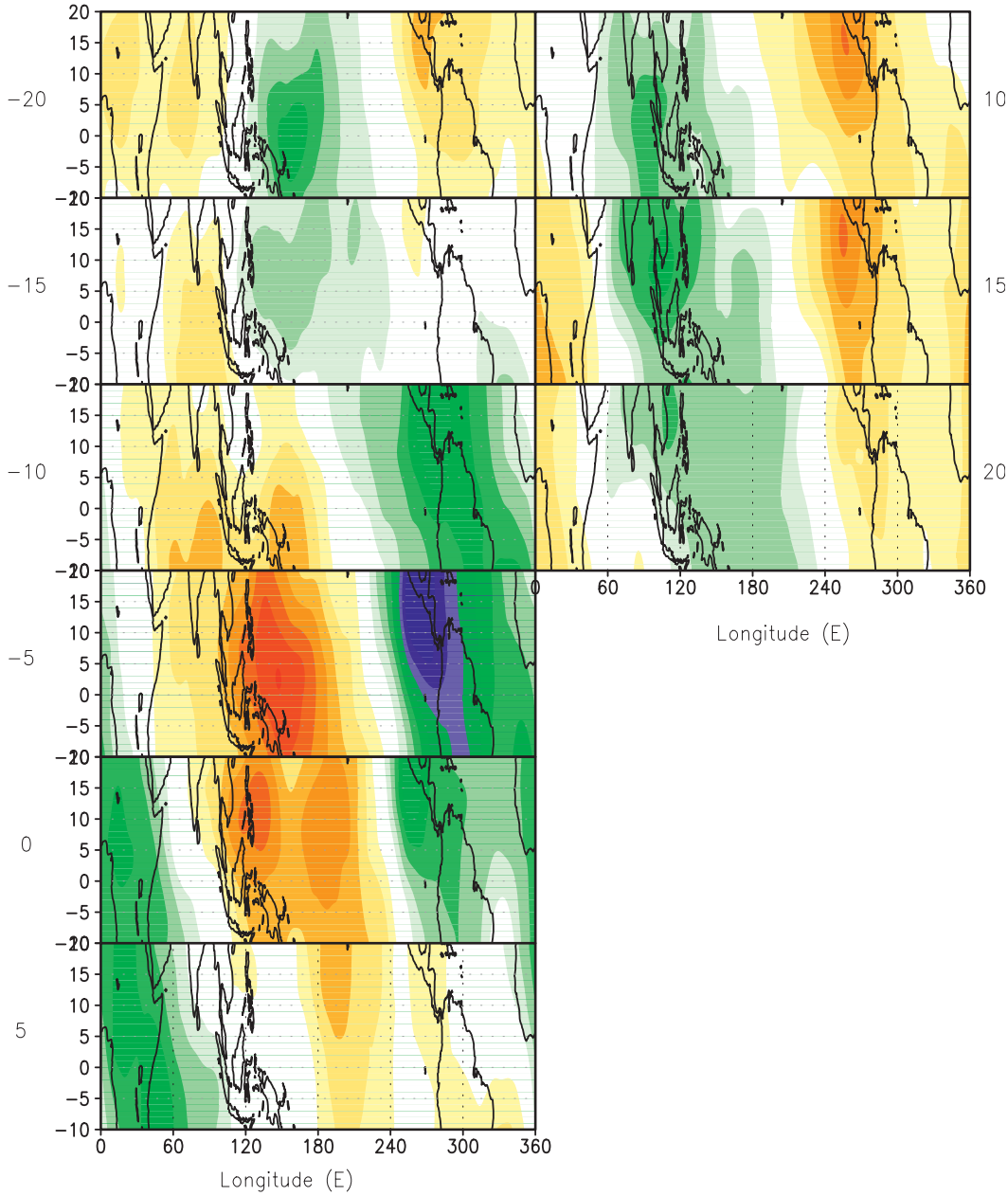

FIG. 15. Composites of velocity potential (10^6 m^2 s^{-1}) at 200 hPa based on ERA-40 data (1980–2001). Data have a 20–90-day filter applied. The plotting time interval is 5 days.

Caribbean and Gulf of Mexico, providing a favorable environment for the further development of the 3–8- and 10–15-day systems entering the region from the east.

Figure 17 summarizes the relationships between the 20–90-day variability and 3–8-day and 10–15-day variability. Here we composite the 20–90-day filtered fields based on the higher frequency (either 3–8 or 10–15 days) indices at 22°N, 110°W. For example, in Fig. 17a, the thick solid line is the usual lagged composite of the 850-hPa moisture flux based on periods when the 3–8-day flux at 22°N, 110°W at day 0 exceeds one standard deviation. In this case, however, we also composite the 20–90-day values using the same 3–8-day flux index. This allows us to examine the low frequency environment associated with the development of the 3–8-day variability. The analogous calculation is done for the 10–15-day variability (Fig. 17b). One further difference from our previous composites is that

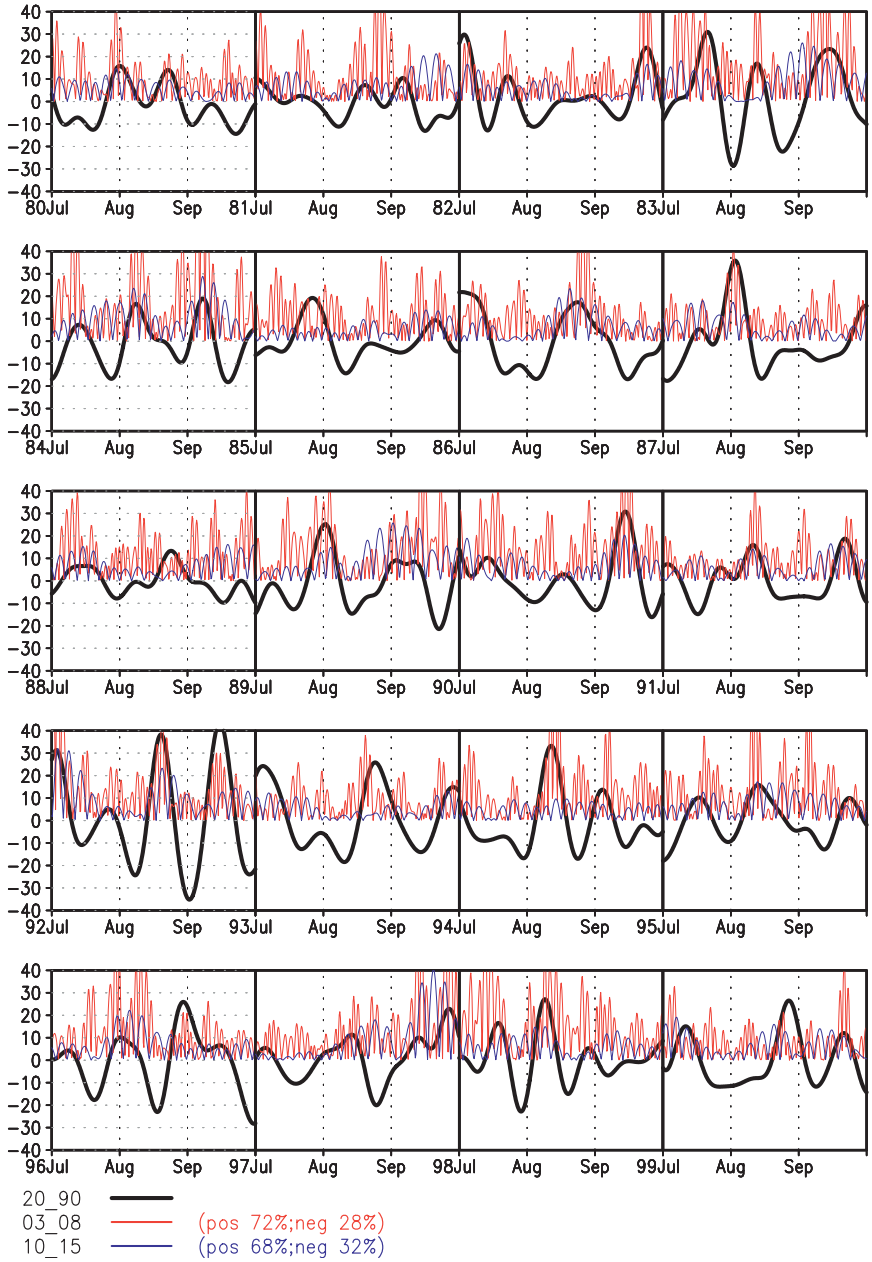

FIG. 16. The vq_{850} (g kg^{-1} m s^{-1}) at 22°N, 110°W from ERA-40 data (1980–2001). The heavy black lines have 20–90-day filter applied. The red lines are the square root of the squared fluxes of the 3–8-day filter data. The blue lines are the same as the red lines, except for the 10–15-day filter data.

all values are plotted as area averages over the region (14°–20°N, 115°–105°W).

The results show that both 3–8-day and the 10–15-day systems tend to preferentially grow in the presence of a (slowly evolving) environment that is characterized by tendencies for increased low-level westerlies, easterly vertical shear, enhanced low-level moisture, rising motion, and decreased surface pressure. The main difference between the two systems is that the 10–15-day systems appear to be less dependent on having low-level westerlies and easterly shear during the development phase. In fact, the shear tends to be westerly and the low-level winds easterly during the early development of these systems. We note that there is a small SST signal in both cases (not shown), with slightly warm anomalies (maximum of about 0.05°C) at −10 days,

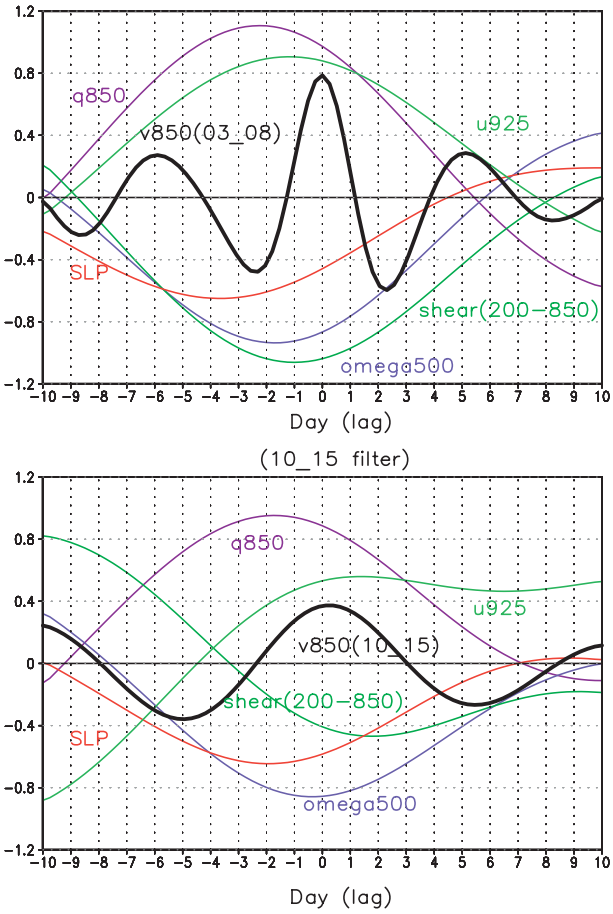

FIG. 17. Composites of various quantities based on an index of (top) 3–8-day filtered and (bottom) 10–15-day filtered vq_{850} at 22°N, 110°W from ERA-40 data (1980–2001). In (top) the heavy black line is the 3–8-day filtered v850 (m s^{-1}) and in (bottom) the heavy black line is the 10–15-day filtered v_{850} (m s^{-1}). The thin lines show various quantities [$q_{850\text{hPa}}$ (g kg^{-1}), vertical motion or ω_{500} (hPa s^{-1}), SLP (hPA), 200–850-hPa shear (m s^{-1}), $u_{925\text{ hPa}}$ (m s^{-1})] that have been filtered to retain time scales of 20–90 days and composited on either the 3–8-day index (top) or the 10–15-day index (bottom). All values are area averages over the region (14°–20°N, 115°–105°W). For plotting purposes, some quantities have been scaled (divided) by the following values: q_{850}: 0.5; ω_{500}: 0.03; 200–850-hPa shear: 2.0; v_{850}: 2.0.

gradually decreasing and turning to cold anomalies of comparable (0.05°C) magnitude by day +10. The warm anomalies are slightly larger and persist somewhat longer for the 10–15-day systems.

The presence of westerly anomalies during the development of the systems is consistent with Maloney and Hartmann (2001), who showed that low-level barotropic energy conversions during westerly MJO periods can provide a significant source of eddy kinetic energy in the eastern Pacific. The results are also consistent with Lorenz and Hartmann (2006), as well as with the work of Maloney and Hartmann (2000) and Molinari and Vollaro (2000), who showed that the convectively active phase of the MJO in the eastern Pacific and Caribbean creates an environment favorable for tropical cyclogenesis. We note that the west-northwestward propagation of these systems in an easterly shear environment is consistent with an interpretation of these systems as moist equatorial Rossby waves (Kikuchi and Wang 2009).

4. Discussion and conclusions

It has long been recognized that the southerly flux of moisture in the Gulf of California is an importance source of the water vapor that feeds summer precipitation over the southwestern United States (e.g., Bryson and Lowry 1955). These fluxes consist of both short-term surges (e.g., Fuller and Stensrud 2000) and longer periods of enhanced mean southerly flow (e.g., Douglas 1995). The connections of these fluxes to the larger-scale flow are not fully understood, though there is considerable evidence from previous studies that easterly waves play an important role (e.g., Stensrud et al. 1997). Previous studies also suggest that the MJO may be important (e.g., Molinari and Vollaro 2000; Higgins and Shi 2001; Lorenz and Hartmann 2006).

In this study, we have taken a broader look at the full range of intraseasonal variability of the flux of moisture entering the Gulf of California. We used the ERA-40 data to examine both spatial structure and primary time scales of the fluxes using a compositing technique that is keyed on the low-level moisture fluxes into the gulf. The results show that the fluxes have a rich spectrum of variability with associated well-defined synoptic and larger-scale circulation features that evolve over a period of several days to several weeks. In particular, we have confirmed and further elucidated the link between enhanced transport over the Gulf of California and 1) African easterly waves on subweekly (3–8 day) time scales, 2) the MJO at intraseasonal time scales (20–90 day), and 3) intermediate (10–15 day) time-scale disturbances that appear to originate primarily in the Caribbean Sea–western Atlantic Ocean.

Our composite analysis describes a canonical link with easterly waves that track across the Atlantic and, upon reaching Mexico, are disrupted and then redevelop on the Pacific coast, finally moving to the northwest to contribute to the moisture flux into the Gulf of California. The enhanced southerly fluxes into the Gulf on these time scales tend to be synchronized with a midlatitude short-wave trough over the U.S. West Coast [consistent with previous findings by Fuller and Stensrud (2000)] and enhanced low-level southerly fluxes over the U.S. Great Plains.

On the intermediate (10–15 day) time scales, we found evidence for contributions to the fluxes from coherent systems that appear to be initiated in the Caribbean Sea or western Atlantic. These systems have zonal wavelengths roughly twice that of the easterly waves, and their initiation appears to be linked to an extratropical U.S. East Coast ridge and associated northeasterly winds that extend well into the Caribbean Sea during their development phase. Tropical systems that appear to be similar to those described here have recently been analyzed by Kikuchi and Wang (2009) and appear to be related to convectively coupled Rossby waves.

On 20–90-day time scales, enhanced low-level westerlies and large-scale rising motion associated with the MJO provides an environment that favors large-scale cyclonic development near the west coast of Central America that, over the course of about two weeks, expands northward along the coast, eventually reaching the mouth of the Gulf of California where it acts to enhance the southerly moisture flux in that region. This development, which appears to be part of a Rossby wave response, includes a northward shift in the eastern Pacific ITCZ, enhanced precipitation over much of Mexico and the southwestern United States, and enhanced southerly/southeasterly fluxes from the Gulf of Mexico into Mexico and the southwestern and central United States. The MJO also has an important impact on the shorter time-scale fluxes (especially on 3–8-day time scales), which tend to have enhanced amplitudes when the convectively active phase of the MJO is situated over the Americas. In that case the MJO provides environmental tendencies characterized by enhanced low-level moisture, increases in low-level westerlies, easterly vertical shear, rising motion, and decreased surface pressure.

Acknowledgments. This work was supported by the NASA Earth Science Enterprises' Global Modeling and Analysis Program. However, Dr. Norden E. Huang is supported in part by a grant from National Research Council, Taiwan (NSC 95-2119-M-008-031-MY3).

REFERENCES

Adams, D. K., and A. C. Comrie, 1997: The North American monsoon. *Bull. Amer. Meteor. Soc.,* **78,** 2197–2213.

Adang, T. C., and R. Gall, 1989: Structure and dynamics of the Arizona monsoon boundary. *Mon. Wea. Rev.,* **117,** 1423–1438.

Badan-Dangon, A., C. E. Dorman, M. A. Merrifield, and C. D. Winant, 1991: The lower atmosphere of the Gulf of California. *J. Geophys. Res.,* **96,** 877–896.

Brenner, I. S., 1974: A surge of maritime tropical air—Gulf of California to the southwestern United States. *Mon. Wea. Rev.,* **102,** 375–389.

Bryson, R., and W. P. Lowry, 1955: Synoptic climatology of the Arizona summer monsoon. Department of Meteorology, University of Wisconsin Scientific Rep. I, 29 pp.

Burpee, T. W., 1975: Some features of synoptic-scale waves based on compositing analysis of GATE data. *Mon. Wea. Rev.,* **103,** 921–925.

Carleton, A. M., 1986: Synoptic-dynamic character of 'bursts' and 'breaks' in the south-west U.S. summer precipitation singularity. *Int. J. Climatol.,* **6,** 605–623.

Douglas, M. W., 1995: The summertime low-level jet over the Gulf of California. *Mon. Wea. Rev.,* **123,** 2334–2347.

——, and J. C. Leal, 2003: Summertime surges over the Gulf of California: Aspects of their climatology, mean structure, and evolution from radiosonde, NCEP reanalysis, and rainfall data. *Wea. Forecasting,* **18,** 55–74.

Fuller, R. D., and D. J. Stensrud, 2000: The relationship between tropical easterly waves and surges over the Gulf of California during the North American monsoon. *Mon. Wea. Rev.,* **128,** 2983–2989.

Green, C. R., and W. D. Sellers, Eds., 1964: *Arizona Climate*. University of Arizona Press, 503 pp.

Hales, J. E., 1972: Surges of maritime tropical air northward over the Gulf of California. *Mon. Wea. Rev.,* **100,** 298–306.

Higgins, R. W., and W. Shi, 2001: Intercomparison of the principal modes of interannual and intraseasonal variability of the North American Monsoon System. *J. Climate,* **14,** 403–417.

——, ——, and C. Hain, 2004: Relationships between Gulf of California moisture surges and precipitation in the southwestern United States. *J. Climate,* **17,** 2983–2997.

Huang, N. E., and S. S. P. Shen, 2005: *Hilbert–Huang Transform and Its Applications*. World Scientific, 311 pp.

——, and Z. Wu, 2008: A review on Hilbert–Huang transform: Method and its applications to geophysical studies. *Rev. Geophys.,* **46,** RG2006, doi:10.1029/2007RG000228.

——, and Coauthors, 1998: The empirical mode decomposition and the Hilbert spectrum for nonlinear and non-stationary time series analysis. *Proc. Roy. Soc. London,* **454A,** 903–995.

——, Z. Shen, and S. R. Long, 1999: A new view of nonlinear water waves—The Hilbert spectrum. *Annu. Rev. Fluid Mech.,* **31,** 417–457.

Kaiser, G., 1994: *A Friendly Guide to Wavelets*. Birkhäuser, 300 pp.

Kalnay, E., and Coauthors, 1996: The NCEP/NCAR 40-Year Reanalysis Project. *Bull. Amer. Meteor. Soc.,* **77,** 437–471.

Keinert, F., 2003: *Wavelets and Multiwavelets*. Vol. 42, *Studies in Advanced Mathematics,* Chapman and Hall/CRC, 288 pp.

Kikuchi, K., and B. Wang, 2009: Global perspective of the quasi-biweekly oscillation. *J. Climate,* **22,** 1340–1359.

Lorenz, D. J., and D. L. Hartmann, 2006: The effect of the MJO on the North American monsoon. *J. Climate,* **19,** 333–343.

Madden, R. A., and P. R. Julian, 1972: Description of global-scale circulation cells in the tropics with a 40–50 day period. *J. Atmos. Sci.,* **29,** 1109–1123.

Maloney, E. D., and D. L. Hartmann, 2000: Modulation of eastern North Pacific hurricanes by the Madden–Julian oscillation. *J. Climate,* **13,** 1451–1460.

——, and ——, 2001: The Madden–Julian oscillation, barotropic dynamics, and North Pacific tropical cyclone formation. Part I: Observations. *J. Atmos. Sci.,* **58,** 2545–2558.

——, and J. T. Kiehl, 2002: MJO-related SST variations over the tropical Pacific during Northern Hemisphere summers. *J. Climate.,* **15,** 675–689.

McCollum, D., R. Maddox, and K. Howard, 1995: Case study of a severe mesoscale convective system in central Arizona. *Wea. Forecasting,* **10,** 643–665.

Molinari, J., and D. Vollaro, 2000: Planetary- and synoptic-scale influences on eastern Pacific tropical cyclogenesis. *Mon. Wea. Rev.,* **128,** 3296–3307.

——, D. Knight, M. Dickinson, D. Vollaro, and S. Skubis, 1997: Potential vorticity, easterly waves, and eastern Pacific tropical cyclogenesis. *Mon. Wea. Rev.,* **125,** 2699–2708.

Oppenheim, A. V., and R. W. Schafer, 1975: *Digital Signal Processing*. Prentice-Hall, 585 pp.

Reed, R. J., D. C. Norquist, and E. E. Recker, 1977: The structure and properties of African wave disturbances as observed during phase III of GATE. *Mon. Wea. Rev.,* **105,** 317–333.

Smith, W. P., and R. L. Gall, 1989: Tropical squall lines of Arizona monsoon. *Mon. Wea. Rev.,* **117,** 1553–1569.

Stensrud, D. J., R. L. Gall, and M. K. Norquist, 1997: Surges over the Gulf of California during the Mexican monsoon. *Mon. Wea. Rev.,* **125,** 417–437.

Uppala, S. M., and Coauthors, 2005: The ERA-40 Re-Analysis. *Quart. J. Roy. Meteor. Soc.,* **131,** 2961–3012.

Vera, C., and Coauthors, 2006: Toward a unified view of the American monsoon systems. *J. Climate,* **19,** 4977–5000.

Wu, M.-L. C., S. D. Schubert, and N. E. Huang, 1999: The development of the South Asian summer monsoon and the Intraseasonal Oscillation. *J. Climate,* **12,** 2054–2075.

——,——, M. J. Suarez, P. J. Pegion, and D. E. Waliser, 2006: Seasonality and meridional propagation of the MJO. *J. Climate,* **19,** 1901–1921.

Zehnder, J. A., D. M. Powell, and D. L. Ropp, 1999: The interaction of easterly waves, orography, and the intertropical convergence zone in the genesis of eastern Pacific tropical cyclones. *Mon. Wea. Rev.,* **127,** 1566–1585.